On the Chronology and Development of Europe's Highest Aeolian Landform: The Sarykum Dune Complex in the North Caspian Region

Dmitry Zastrozhnov[1,2,*], Andrey Zastrozhnov[1], Sergei Medvedev[2,3,4], Idris Idrisov[5], Viktor Spiridonov[1,6], Dmitry V. Nazarov[1]

[1]*Russian Geological Research Institute, Saint Petersburg, Russian Federation*

[2]*University of Oslo, Department of Geosciences, Oslo, Norway*

[3]*Volcanic Basin Energy Research, Oslo, Norway*

[4]*Medvedev Consulting, Oslo, Norway*

[5]*Institute of Geology, Dagestan Scientific Centre, Russian Academy of Sciences, Makhachkala, Russian Federation*

[6]*Russian Oil Research Institute (VNIGNI), Moscow, Russian Federation*

**corresponding author: zastrozhe@gmail.com*

Abstract

The highest aeolian landform in Europe, the Sarykum dune complex, is located in the southwestern Caspian Depression near the Caucasus Mountains. Despite its prominence and accessibility, its morphology and evolution have been previously poorly understood. In this study we investigate the dune complex through a synthesis of geomorphological, geological, and geochronological methods. Our findings link its development to climatic aridification driven major regression phases of the Caspian Sea during the Late Pleistocene–Holocene. Optical stimulated luminescence dating indicates that dune formation began at least 70 ka during the Atelian regression, with reactivation around 12–8 ka during the Mangyshlak regression. By the early Holocene, the complex had nearly reached its modern height. The Shura-Ozen’ River, which divides the dune complex in two major segments, played a significant role in the complex’s evolution, influencing aeolian sediment transport and trapping material on its banks, particularly on the left bank, where the highest Central Massif is located. Extensive vegetation now stabilizes most of the complex, except for active ridges in the Central Massif. A numerical analysis of wind potential for dune migration, based on meteorological data spanning the past 55 years, shows that sand movement is primarily driven by self-sustaining NW–SE wind fluctuations. Paleowind analysis suggests that similar long-term wind patterns have persisted since the onset of aeolian deposition during the Atelian phase. Our multidisciplinary study sheds new light on the Sarykum dune complex's history and highlights

its significance as a dynamic archive of climatic and geomorphic processes in the Caspian region.

1. Introduction

Fluctuations in the Caspian Sea level and associated climatic changes have played a significant role in the desertification of coastal regions during the Late Pleistocene-Holocene (e.g., Leroy et al., 2021; Volozh et al., 2022). Understanding the temporal and spatial conditions of these past climatic events is essential for predicting and modeling the future development of landscapes and the environment in the Caspian region, particularly in light of ongoing global climate changes (e.g., Koriche et al., 2021a, 2021b). This is especially important for the Caspian Depression, a vast, low-lying area in the North Caspian region (Fig. 1), which is particularly sensitive to even subtle sea level fluctuations in the Caspian Sea. Although evidence of these climatic events is often preserved in the sedimentary record of the North Caspian region, their geological interpretations have often been subject to debate due to conflicting sedimentological and geochronological results (e.g., Fedorov, 1957, 1978; Popov, 1983; Rychagov, 1997; Svitoch and Yanina, 1997; Svitoch and Klyuvitkina, 2006; Yanina, 2009; Richards et al., 2014; Badyukova, 2021; Költringer et al., 2021; Zastrozhnov et al., 2021, 2024).

Located at a greater distance from modern deserts (Fig. 1a), the Sarykum dune complex represents a unique example of a large isolated aeolian landform, which may serve as a geological reference object for studying desertification processes in the North Caspian region throughout the Late Pleistocene-Holocene. The Sarykum dune complex is the highest aeolian landform in Europe and one of the highest in Eurasia (e.g., Gusarov, 2016; Balykova and Andreeva, 2023). Situated in the southwest part of the Caspian Depression, near its junction with the Caucasus Mountains (Figs. 1, 2, 3), the complex lies within a dynamic environmental setting where aeolian, marine, fluvial, and tectonic processes closely interact. The formation and development of the Sarykum dune complex were hypothesized to be associated with Late Pleistocene-Holocene epochs of aridization and humidification, closely tied to significant fluctuations in the Caspian Sea level (Idrisov, 2010).

Despite first being scientifically described more than a century ago (Barbot de Marny, 1894; Maiorov, 1927), the Sarykum dune complex remained poorly studied until recent decades, when new factual material on its morphology, structure, and sedimentology has been published (e.g., Idrisov, 2010; Gusarov, 2014, 2015, 2016; Gusarov et al., 2016; Matsapulin et al., 2013, 2021; Balykova and Andreeva, 2023). Nonetheless, the chronology of development of the complex remains missing, preventing a reliable correlation with regional climatic events. An ongoing debate persists regarding the origin and source of the sand material comprising the complex (e.g., Idrisov, 2010; Gusarov, 2015). Principal proposed hypotheses include: (1) aeolian erosion and redeposition of pre-Quaternary sandstones from the neighboring mountain ranges (e.g., Barbot de Marny, 1894; Idrisov, 2010); (2) aeolian redeposition of the marine deposits after the Caspian Sea regression (Maiorov, 1927); (3) reworking of thick alluvial fans originating from neighboring mountain ranges (e.g., Gusarov, 2014, 2016); (4) interaction of aeolian and volcanogenic processes (Matsapulin et al., 2013, 2021).

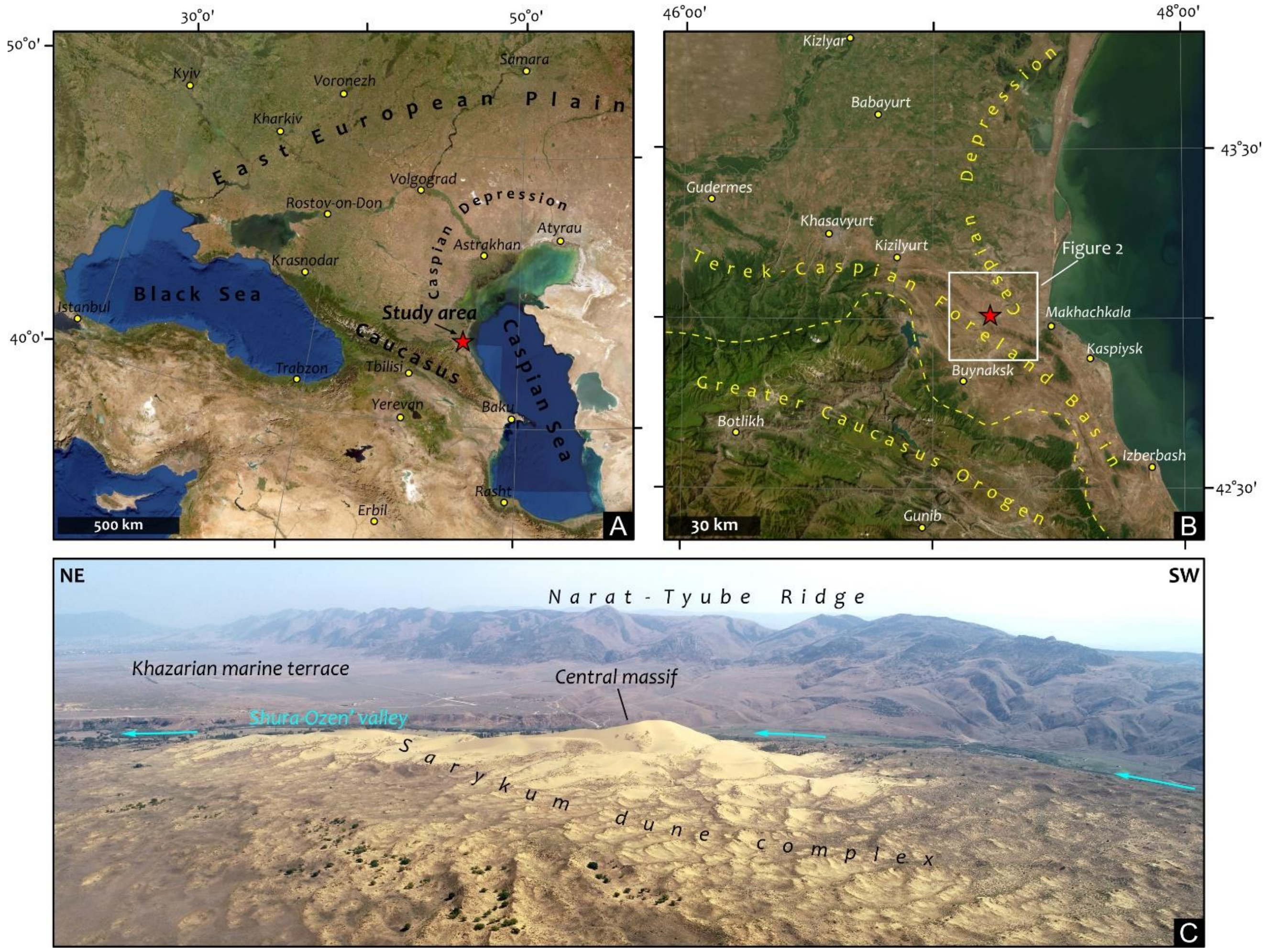

Figure 1. (A) Satellite image of the Ponto-Caspian region showing the location of the study area. (B) Satellite image of the northeastern Caucasus region highlighting the position of the Sarykum dune complex (marked with a red star). Basemap: ArcGIS Imagery. (C) Drone view of the Sarykum dune complex, with the Central Massif in the foreground and the Shura-Ozen' River valley, Khazarian marine terrace, and Narat-Tyube Ridge in the background. View from the NW.

The primary objectives of our study were to establish a chronology for the Sarykum dune complex using optically stimulated luminescence (OSL) dating and to correlate it with regional climatic events; to analyze sedimentary structures to infer paleowind directions and compare them with the modern wind regime; to evaluate the findings in the context of existing hypotheses; and to integrate these insights into a comprehensive formation model.

2. Geological framework

The Sarykum dune complex is located in the Republic of Dagestan, Russian Federation, approximately 18 km northwest of its administrative center, the city of Makhachkala. Positioned at the southwest tip of the Caspian Depression at the border with the Narat-Tyube Ridge of the Caucasus Mountains (Figs. 1b-c, 2, 3), the complex comprises of a NW oriented field of primarily stabilized sand dunes. The complex is divided into two parts, Western and Eastern Sarykum, by the valley of the Shura-Ozen' River. The Shura-Ozen' River cuts through the middle part of the Narat-Tyube Ridge and descends to the plain of the Caspian Depression (Fig. 2). In the western and largest part of the Sarykum dune complex, there is a central sand massif (Central Massif) located right at the riverbank, which is the dominant topographic feature of the complex, rising to 170 meters above the base of the complex and reaching an absolute height of approximately 240 m a.s.l. (Figs. 1c, 4).

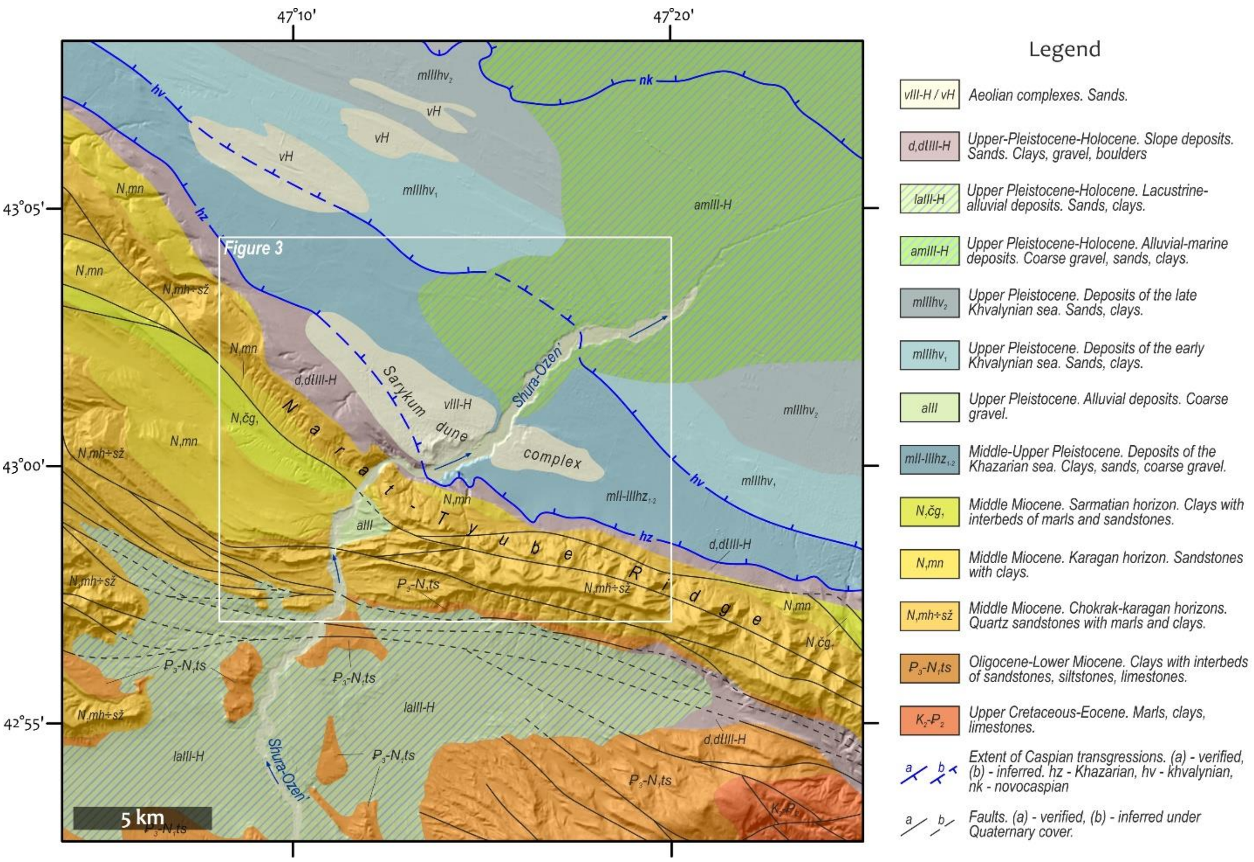

Figure 2. Simplified geological map of the study area (modified after Enna et al., in press), showing the main pre-Quaternary and Quaternary stratigraphic units. The regional extent of this map is indicated in Figure 1b.

The Narat-Tyube Ridge, also referred to as the Narat-Tyube Monocline, is a component of the Terek-Caspian Foreland Basin. This basin formed as a result of flexural subsidence induced by the alpine orogeny of the Greater Caucasus since the Oligocene. The created an accommodation space was filled by a thick pile of sediments, with the lower part of the succession predominantly composed of shales of the Oligocene to Lower Miocene Maikop Group, and the upper part consisting of Middle Miocene to early Quaternary continental molasse. It has also experienced several phases of late Cenozoic compressional reactivations (e.g., Sobornov, 2021 and references therein).

The Narat-Tyube Ridge exposes Middle Miocene (Chokrak-Karagan horizons) deposits, primarily composed of quartz, weakly cemented sandstones, along with subordinated clays and marls (Enna et al., in press). Further north towards the lowland, these Middle Miocene formations are overlain by Middle to Upper Miocene clays of the Sarmatian horizon. The clays of the Sarmatian horizon form the base of the geological section that is outcropped along the banks of the Shura-Ozen’ River within the study area.

Throughout the Pliocene-Quaternary, the Caspian Depression experienced several major epochs of Caspian Sea transgressions and regressions. However, only the sedimentary interval from the Middle-Late Pleistocene to the Holocene is preserved above the Sarmatian clays in the study area. The Sarmatian clays are overlain by marine clayey sands and alluvial-marine coarse gravels, which are believed to have accumulated during the Khazarian transgression of the Caspian Sea (e.g., Fedorov, 1957), which occurred during Marine Isotope Stages 10 to 5 in the Middle-Late Pleistocene. These deposits constitute a body of marine terrace at an altitude of ca. +80-70 m a.s.l., which encircles the foothill of the Narat-Tyube Ridge (Fig. 2). However, it is suggested that the maximum level of the Khazarian transgression was significantly lower, around +35 m a.s.l., and that the modern elevation of this terrace is the result of neotectonic uplift in the region (Idrisov, 2013). The Sarykum dune complex sits on top of this terrace (Fig. 2), indicating that the formation of the complex started no earlier than 80 ka (Idrisov, 2010).

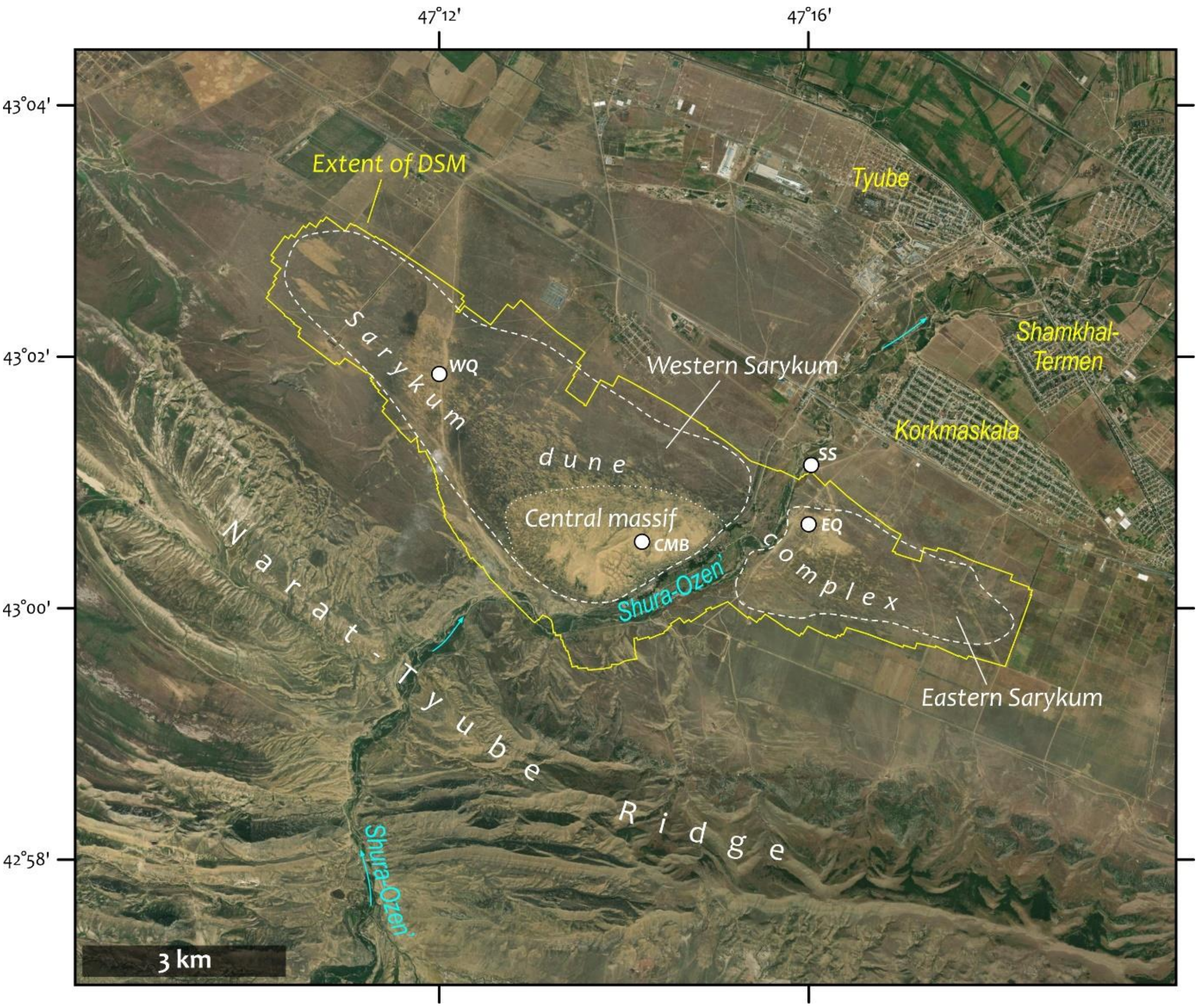

Figure 3. Satellite image of the Sarykum dune complex and the adjoining part of the Narat-Tyube Ridge. Basemap: ArcGIS Imagery. Main studied sites: CMB – blowout in the Central Massif; EQ – eastern quarry; SS –outcrop exposing substratum deposits on the right bank of the Shura-Ozen' River; WQ – western quarry (see Table 1 and section 4.2).

3. Data and methods

3.1. Field data: drone survey and sedimentary structure analysis

In August 2022, we conducted geological field work within the Sarykum dune complex. Using a DJI Phantom 4 Pro+ drone, an aerial survey of the entire dune complex was performed (Figs. 3, 4). The drone was manually operated at an average height of 150 meters above ground level, capturing over 2100 photos with nadir-oriented cameras. These photos underwent processing in Agisoft Metashape software (Agisoft, 2022), following the standardized workflow established by the USGS (Over et al., 2021). This process resulted in the generation of a Digital Surface Model (DSM) and orthophotomosaic with resolution of 27 cm/pixel and

14 cm/pixel, respectively. The DSM and orthophotomosaic cover an overall area of 29 km^2, with the dune complex occupying approximately 20 km^2 (Fig. 3). During the fieldwork, we opted not to use ground control points for efficiency. The georeferencing of the DSM and orthophotomosaic was subsequently quality-checked using global terrain models such as SRTM and Copernicus, ensuring its suitability for the morphological analysis conducted in our study.

An aerial survey was conducted along a quarry located in the eastern part of the dune complex to generate a high-resolution photorealistic Digital Outcrop Model (DOM). A total of 63 photos were processed in Agisoft Metashape to create a DOM of the quarry with a resolution of 1 cm/pixel. The DOM was then utilized to describe the internal structure of the aeolian succession and to perform geological measurements, including the thickness of the units and bedding orientations. The geological measurements and interpretation of the DSM and DOM were done in Agisoft Metashape (Agisoft, 2022) and LIME software (Buckley et al., 2019).

To determine the sediment transport direction, we measured cross-bedding series orientations in key localities of the dune complex (Table 1). These localities included quarries in the western and eastern parts of the complex, as well as a blowout at the top of the Central Massif (Fig. 3).

Table 1. Position and coordinates of the main studied localities within the Sarykum dune complex.

Locality	Position	Lat	Lon
Substratum sediments (SS)	Right bank of the Shura-Ozen' River, 1.3 km NW of the eastern quarry	43° 1' 16" N	47° 16' 27" E.
Eastern Quarry (EQ)	NW corner of the Eastern Sarykum; NE part of the quarry, N-NW-facing wall	43° 0' 30.9" N	47° 16' 14.8" E
Western Quarry (WQ)	Western part of the Western Sarykum, 3.5 km NW of the Central Massif	43° 1' 49.9" N	47° 11' 59.5" E
Blowout in the Central Massif (CMB)	Small blowout next to the touristic viewpoint, where 4-m thick aeolian succession is outcropped	43° 0' 32.6" N	47° 14' 7.9" E

3.2. OSL dating

We collected 14 samples for OSL dating: 3 samples from the substratum sediments on the right bank of the Shura-Ozen' River, 7 samples from aeolian deposits in the eastern quarry and 4 samples in the blowout near the top of the Central Massif. The samples were collected by hammering steel and plastic tubes (~5*30 cm) into freshly-cleaned sections, and they were subsequently sealed to preserve moisture before being transported to the laboratory. Sample preparation and OSL dating were conducted at the OSL laboratory of the Russian Geological Research Institute.

All samples were prepared by standard methods described by Wintle (1997) under the red light. Quartz equivalent dose (D_e) measurements were done using a Risø TL/OSL Reader DA-20 C/D with the Single Grain OSL attachment module following the single aliquot regeneration (SAR) protocol (Murray and Wintle, 2003) in small aliquots (2 mm) mounted on stainless steel discs. To isolate fast component of quartz OSL signal for equivalent dose estimation was summed over the initial 0.32 s with the early background subtraction. The suitability of the SAR protocol was tested using a dose recovery test for several samples for three aliquots of quartz. D_e values are given as arithmetic average.

Moreover, single grain K-feldspar post-IR IRSL dating (Thiel et al., 2011) using $pIR_{50}IR_{170}$ and $pIR_{50}IR_{290}$ signals were applied to one of the youngest (RGI-1105) and oldest (RGI-1112) samples respectively. Equivalent dose was determined for individual grains each spaced in a sample hole on standard aluminum single-grain disc. Single grain measured signal was summed over the initial 0.17 s of the decay curve and subtracting the signal from a late background, taken from 0.34 s. Anomalous fading tests were made for each of two samples and show average g-value 1.0±1.5 %/decade for RGI-1105 and 0.5±0.8 %/decade for RGI-1112. D_e values are given as arithmetic mean with no fading correction.

Activities of 226Ra, 232Th and 40K were determined using high-resolution gamma spectrometer with a high purity germanium (HPGe) detector Canberra BE3825 after sealing each sample with wax and storing it for a minimum of 20 days to allow for radon re-equilibrium. Dose rates were calculated using the conversion factor from Guérin et al. (2011) and dose cosmic rates according to Prescott and Hutton (1994).

3.3. Wind data analysis

Wind data specific to the Sarykum dune complex is unavailable; therefore, we utilized wind direction and speed data from the nearest meteorological station in Makhachkala. This data, covering 1966 to 2023, was obtained from the “Russian Research Institute of Hydrometeorological Information - World Data Center” through an online database (Bulygina et al., 2014). Observations were recorded at standard synoptic times in 3-hour intervals, with wind speeds analyzed in meters per second (m/s).

Despite much of the Sarykum dune complex currently being vegetated and therefore resistant to aeolian reworking, we applied the method proposed by Fryberger and Dean (1979) to evaluate the magnitude and direction of potential aeolian sediment transport under the recent wind regime and to compare it with possible paleowind regimes. Here, we reformulate the classical description of the method using the vector approach and adopt the possibility of method applications to subsets of measurements. Each *j*-th wind measure (wind vector $\vec{V_j}$ characterized by certain direction and speed V_j) is converted to elementary drift potential which is a vector

$$\overrightarrow{DP_j} = \begin{cases} \vec{V_j} \cdot V_j\left(V_j - V^*\right), & V_j > V^* \\ 0, & V_j \leq V^* \end{cases} \qquad (1)$$

This vector is codirected with the wind vector $\vec{V_j}$ and has length $\left|\overrightarrow{DP_j}\right|$ (termed hereafter as DP_j). The threshold wind velocity (V^*) is the minimum wind speed at 10-m height required to initiate sand movement. In our calculations, we applied a threshold velocity of 6.5 m/s, which is sufficient to mobilize sand grains of 0.35-0.4 mm in diameter (Bagnold, 1941), aligning with the typical grain size of the Sarykum sands (Gusarov, 2016). Notably, only 13.5% of all wind measurements exceed 6.5 m/s, resulting in non-zero DP_j values. We also checked values between 4 and 9 m/s for V^* to ensure that further conclusions are independent of chosen criterion.

The Drift Potential (*DP*) as defined by Fryberger and Dean (1979) can be assigned as a weighted average of lengths of elementary drift potentials (eq. 1) with weights equal to the fraction time of each individual measurement. The data used here has equal time spacing and thus we adopt a simple averaging of a set *A* of *N* measurements:

$$DP = \frac{1}{N}\sum_{j \in A} DP_j \qquad (2)$$

Traditionally, the *DP* is based on the set *A* equal to the total set of observations (and *N*=168959). In this study, to understand a dynamics of wind forcing, we also calculate *DP* for subsets of measurements. For example, eq. 2 for subset “year 1966” uses *A*={1, 2,…, 2921} and *N*=2921. This approach can also help analyze seasonal variations, calculating and comparing *DP* for certain groups of months for the entire observation time.

Based on studies of various deserts, Fryberger and Dean (1979) proposed a classification of wind-energy environments according to *DP* values. While the original classification used wind velocities measured in knots, here we apply the recalibration based on wind velocities measured in m/s (Bullard, 1997). In this adjusted classification, a low-energy environment is characterized by *DP* values below 27, an intermediate-energy environment by *DP* values of 27-54, and a high-energy environment by *DP* values exceeding 54.

In addition to scalar average (eq. 2) we introduce vector average of elementary drift potential (eq. 1). We term it as a vector Resultant Drift Potential ($\overrightarrow{RDP}$):

$$\overrightarrow{RDP} = \frac{1}{N}\sum_{j\in A}\overrightarrow{DP_j} \qquad (3)$$

Following Fryberger and Dean (1979) parameters Resultant Drift Potential (*RDP*) and Resultant Drift Direction (*RDD*) are the length and direction of vector $\overrightarrow{RDP}$ respectively. Note the importance of direction of $\overrightarrow{DP_j}$ in eq. 3. For example, two elementary drift potentials of unit length and opposite directions result in scalar average (eq. 2) *DP*=1, while eq. 3 results in a vector of zero length.

Similar to eq. 2, eq. 3 can use the total set of measurements as well as a desired subset of those. The accurate vector summation in eq. 3 avoids the biases associated with bin-distribution methods, as it directly incorporates each individual data point without preordering (cf., Pearce and Walker, 2005).

The *RDP/DP* ratio reflects the directional consistency of the wind regime. *RDP/DP* close to 1 indicates unidirectional winds, while values approaching zero suggest winds from multiple directions, as the *RDP* becomes low (Fryberger and Dean, 1979).

4. Results

4.1. General structure and morphology

4.1.1. Eastern Sarykum

The eastern part of the complex is lower compared to the western part, with the lowest altitude around 65 m a.s.l. in the easternmost part of the complex (Fig. 4). The height of the Eastern Sarykum increases towards the Shura-Ozen’ valley, reaching around 100-110 a.s.l. near the eastern quarry (Fig. 4). The current structure and morphology of the entire Sarykum dune complex is influenced by its vegetation cover (Fig. 1c), which stabilizes sand transportation. The Eastern Sarykum displays a “pockmarked” type of topography, as defined by Barchyn and Hugenholtz (2013), where many blowouts develop on pre-existing sand deposits, but their advancement is quickly stabilized by vegetation and does not lead to the formation of pronounced parabolic dunes.

On the periphery of the Eastern Sarykum, both saucer- and trough-shaped blowouts typically occur, oriented in a NW-SE direction, with depositional lobes locally recognizable on either their NW or SE sides, or on both sides (Fig. 5a). The blowouts are typically 30 to 80 meters long (locally over 150 meters), 20 to 50 meters wide, and 3 to 7 meters deep.

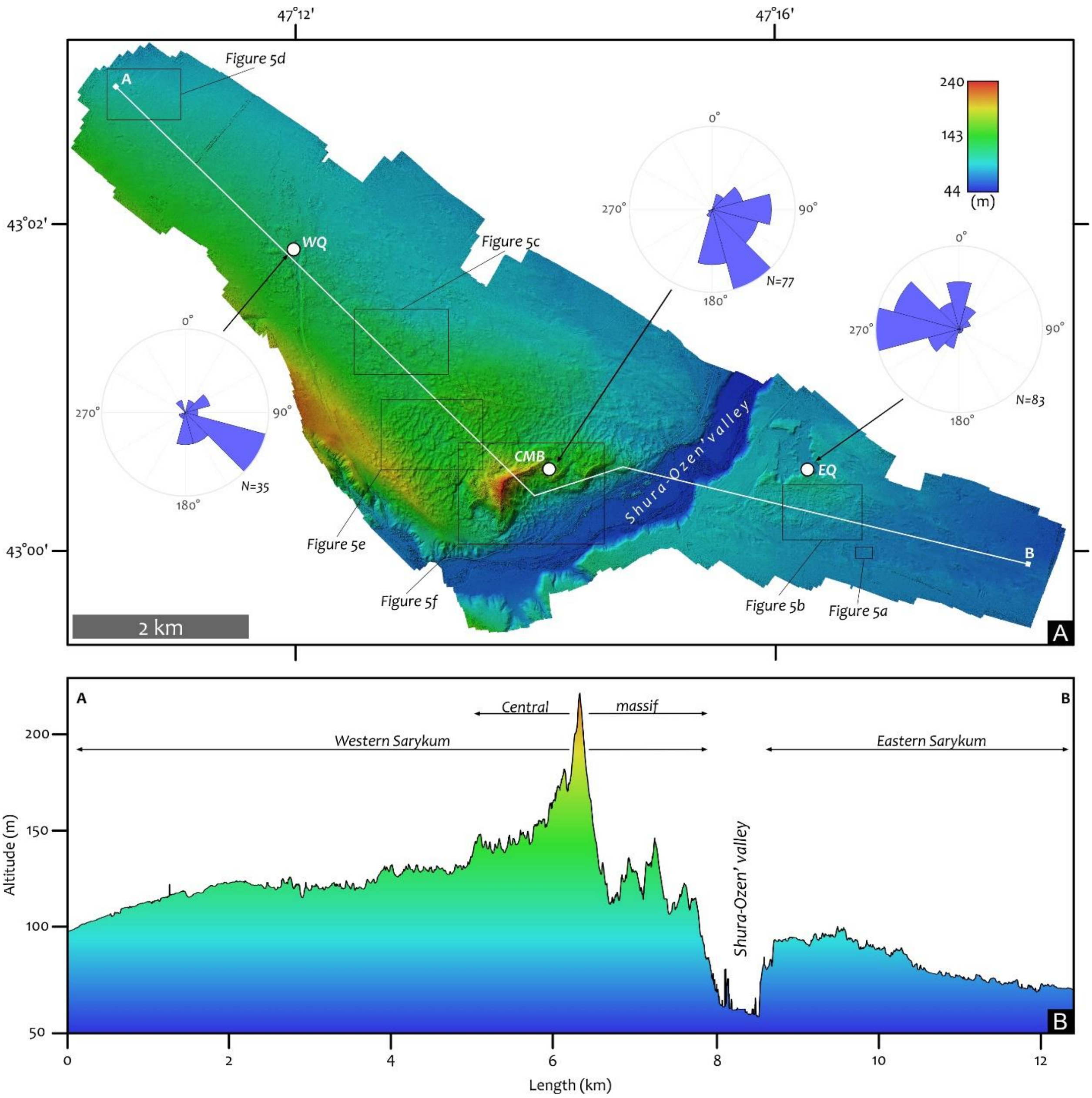

Figure 4. (A) High-resolution Digital Surface Model of the Sarykum dune complex. Rose diagrams indicate the dip directions of cross-sets measured in aeolian deposits at the main studied sites: CMB – blowout in the Central Massif; EQ – eastern quarry; WQ – western quarry. The extent of the model is shown in Figure 3. (B) Elevation profile A-B across the Sarykum dune complex, highlighting its main morphological segments. See the location of the profile in Figure 4A.

The highest and thickest part of the Eastern Sarykum displays a much more complex and ridged morphology. These ridges represent a complex network of erosional walls of blowouts, which also tend to orient in a NW-SE direction (Fig. 5b). There are also minor unvegetated patches where local deflation forms active blowouts and short-distance sand transportation can still occur. Additionally, the active quarry area in the eastern part of the complex is prone to aeolian reworking, which redeposits sand material primarily along the quarry walls.

4.1.2. Western Sarykum and Central Massif

The western part forms the highest section of the dune complex, with the Central Massif reaching around 240 m a.s.l. at its peak (Fig. 4). The lowest, northern segment of the Western Sarykum, off the Central Massif, lies at an altitude of 80-90 m a.s.l. Towards the Narat-Tyube Ridge and Central Massif, the altitude of the complex increases, with an average height of around 120-160 m a.s.l. (Fig. 4a)

Off the Central Massif, the structure and morphology of the Western Sarykum is similar to that of the Eastern Sarykum, displaying a “pockmarked” topography with many blowouts (Fig. 5c). In contrast to the Eastern Sarykum, a significant part of the blowouts in the Western Sarykum are currently unvegetated and reactivated by wind erosion. Both active and stabilized blowouts are saucer- and trough-shaped, oriented in a NW-SE direction. They are typically 30 to 60 meters long, 10 to 40 meters wide, and 2 to 7 meters deep. In the westernmost part, some of the blowouts can exceed 200 meters in length and 90 meters in width. Depositional lobes are developed on both NW and SE sides; however, in active blowouts, they are better developed on the SE sides. In large blowouts in the westernmost part, depositional lobes may evolve into prominent sand sheets, which can prograde over 300 m in a SE direction, although the distal portions of these sand sheets are partially vegetated. (Fig. 5d).

At the western and northern foot of the Central Massif, vegetation still prevents massive sand transportation, yet the morphology of the dune complex changes remarkably. Here, it is mainly represented by weakly pronounced relict sand ridges, which are oriented in NE-SW direction and associated with rake-like en-echelon blowouts (Fig. 5e). These blowouts are dominantly saucer-shaped, typically 20 to 40 meters long, 15 to 30 meters wide, and 3 to 7 meters deep, with long axes oriented in a NW-SE direction and depositional lobes primarily developed on the SE sides.

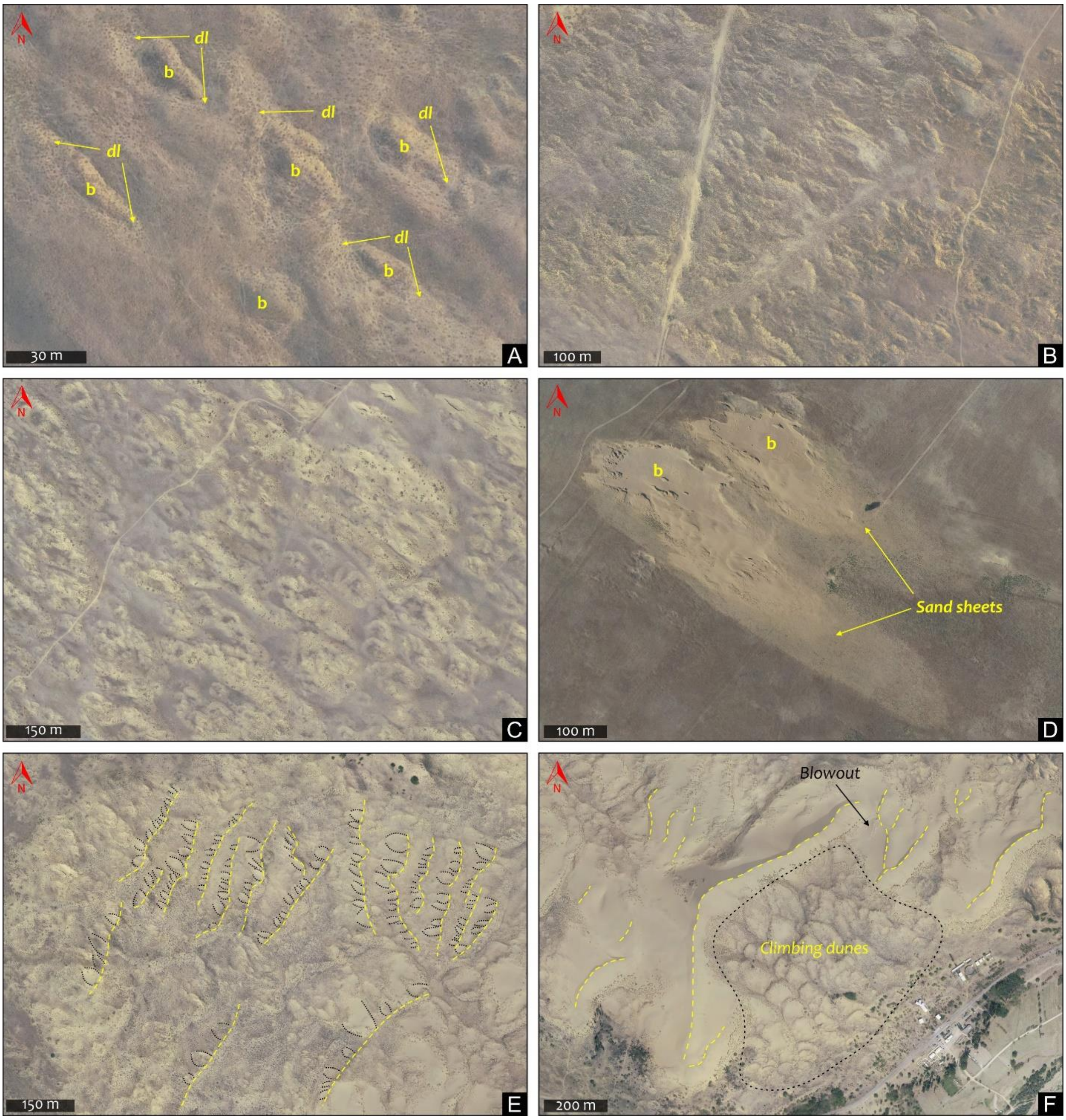

Figure 5. Fragments of the high-resolution orthophotomosaic illustrating the main morphological features of the Sarykum dune complex: (A) NW-SE oriented blowouts (b) and depositional lobes (dl) on their sides in the Eastern Sarykum; (B) ridged morphology of the Eastern Sarykum, featuring a complex network of erosional walls within blowouts; (C) “pockmarked” topography of the Western Sarykum, with many partly reactivated NW-SE oriented blowouts; (D) large blowouts (b) in the westernmost part of the Western Sarykum, forming sand sheets on their SE sides; (E) fragment of the western part of the Central Massif, showing relict dune ridges (highlighted by yellow dashed lines) modified by rake-like en-echelon blowouts (marked by black lines); (F) central part of the Central Massif, with large active ridges (indicated by dashed yellow lines) and vegetated climbing dunes

developed on the southeastern slope. The position of the studied blowout in the Central Massif is shown. The locations of these figures are shown in Figure 4a.

Towards the highest part of the Central Massif, the absence of vegetation cover promotes the formation of active sand ridges oriented in both N-S and NE-SW directions (Fig. 5f). Most ridges measure between 150 and 350 meters in length, but the largest ridge, which forms the highest point of the complex, stretches 1.1 km in length. This ridge exhibits a sinuous geometry, with its southern segment extending 450 m in a N-S direction, while the northern segment runs in a NE-SW direction (Fig. 5f). As of August 2022, the eastern and southeastern slopes of the ridge are approximately 20 degrees, while the western and northwestern slopes are slightly steeper, at around 30 degrees.

The southeastern slope of the Central Massif, inclined at approximately 15 to 20 degrees, features a distinctive network of climbing dunes. These dunes include compound, imbricated parabolic forms that accrete obliquely to the slope in a N to NE direction (Fig. 5f). They are currently stabilized, with both crests and lee sides being vegetated.

4.2. Internal structure and age of sediments

4.1.1. Substratum

The substratum deposits, which underlie the Sarykum dune complex and form the body of the marine terrace, are most clearly exposed in the study area in the outcrops along the right bank of the Shura-Ozen’ River. The stratigraphy begins with Sarmatian (Middle–Upper Miocene) black clays (Fig. 6), which are slightly deformed and dip toward the N–NE at an angle of 25–30 degrees. These clays have a visible thickness exceeding 20 meters. The top of the Sarmatian clays represents a clear angular unconformity with a stratigraphic gap of over 5 myr, which separates them from the overlying Middle-Late Pleistocene Khazarian sediments. The base of the Khazarian sediments lies here at approximately 65-80 m a.s.l. They consist of alternating layers of sands and clayey sands, rich in marine mollusk shells of Khazarian age and their fragments (e.g., Fedorov, 1957). Coarser pebble-gravel layers (1-1.5 meters thick) become more prominent in the middle part of the layer. The overall thickness of the Khazarian sediments (as defined by Fedorov, 1957) in this area is about 10-15 meters.

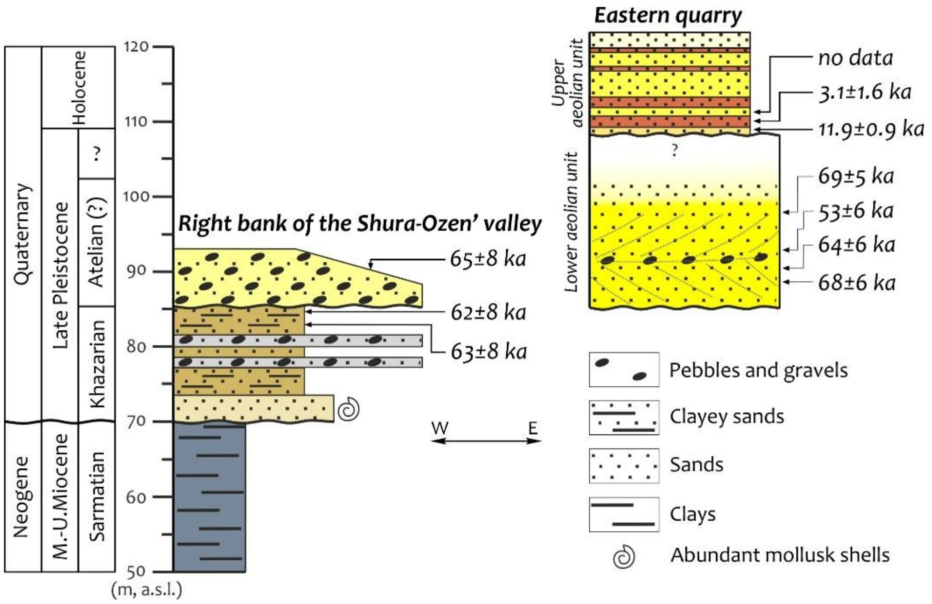

Figure 6. Lithostratigraphic summary of the outcrop on the right bank of the Shura-Ozen' River exposing substratum deposits (SS; stratigraphy after Fedorov, 1957) and the quarry exposing the overlying aeolian units in the Eastern Sarykum (EQ). Only quartz OSL ages are shown. The locations of the sites are shown in Figures 3 and 4a.

The section is topped by a prominent layer, which erosionally rests on the underlying sediments and consists of coarse-grained pebble-gravel deposits interlayered with sands and including rare boulders of sandstones (Figs. 6 and 7). The thickness of this layer is about 3-6 meters, reaching up to 8 meters in some areas. The sands of the Sarykum dune complex lie directly on top of it.

We collected OSL samples from the upper part of the substratum section in a small outcrop on the right bank of the Shura-Ozen' River (Fig. 7b; Table 2), approximately 1.3 km NW of the eastern quarry (Fig. 3; Table 1). A sample taken from the middle of the 3-meter-thick layer of pebble-gravel deposits at the top of the terrace provided a quartz OSL age of 65±8 ka (RGI-1285). In the underlying layer, which consists of horizontally-bedded fine-grained sands with mollusk shell detritus, we obtained two quartz OSL dates: a sample collected 0.5 meters below the top of this layer was dated 62±8 ka (RGI-1284), while a sample taken 5 meters below the top was dated 63±8 ka (RGI-1283).

Table 2. Optically stimulated luminescence (OSL) ages for quartz (Q) and K-feldspar (KF). n_a, n_r and n_{all} are the numbers of accepted for D_e estimation, rejected and all measured quartz aliquots or K-feldspar grains respectively.

Locality	Lab code	w.c. (%)	Specific activity (Bq/kg)				Q				KF			
			^{238}U	^{226}Ra	^{232}Th	^{40}K	na/nr	Dose rate (Gy/ka)	Equivalent dose (Gy)	**Age (ka)**	na/nr/ nall	Dose rate (Gy/ka)	Equivalent dose (Gy)	**Age (ka)**
Substratum sediments: right bank of the Shura-Ozen' River (SS)	RGI-1283	20	20±4	20.7±0.4	18.4±0.3	317±15	8/5	1.46±0.05	93±10	**63±8**				
	RGI-1284	19	34±6	31.5±0.6	24.2±0.5	421±20	7/2	2.07±0.08	128±16	**62±8**				
	RGI-1285	11	39±6	21.8±0.4	13.3±0.3	201±10	9/0	1.39±0.05	90±10	**65±8**				
Eestern Sarykum Quarry (EQ)	RGI-1105	17	12±2	10.5±0.2	8.7±0.2	143±7	9/1	0.83±0.03	56±4	**68±6**	6/18 /300	1.69±0.18	104±10	**62±9**
	RGI-1106	18	13±2	10.6±0.2	9.1±0.2	159±8	9/3	0.90±0.03	58±5	**64±6**				
	RGI-1107	16	13±2	11.3±0.3	9.8±.02	171±9	11/0	0.99±0.04	53±6	**53±6**				
	RGI-1108	18	10±2	9.7±0.2	8.4±0.2	145±8	9/1	0.86±0.03	59±4	**69±5**				
	RGI-1109	16	7±1	5.4±0.1	3.6±0.1	42±3	7/12	0.39±0.01	4.6±0.3	**11.9±0.9**				
	RGI-1110	16	5±1	6.0±0.2	5.0±0.1	95±5	2/11	0.58±0.02	1.8±0.9	**3.1±1.6**				
	RGI-1111	17	6±1	6.2±0.2	5.6±0.1	111±6	5/0	0.63±0.03	-	-				
Blowout in the Central Massif (CMB)	RGI-1112	16	7±1	5.8±0.2	3.6±0.1	40±3	9/4	0.43±0.02	3.4±0.2	**7.9±0.6**	29/1 /300	1.30±0.18	10.6±0.5	**8.2±1.2**
	RGI-1113	17	5±1	5.9±0.2	3.8±0.1	46±6	7/6	0.45±0.02	3.9±0.3	**8.7±0.8**				
	RGI-1114	17	6±1	5.4±0.2	3.9±0.1	51±3	9/8	0.48±0.02	3.9±0.2	**8.1±0.6**				
	RGI-1115	17	6±1	5.4±0.2	3.7±0.1	43±3	8/8	0.48±0.02	3.4±0.2	**7.0±0.5**				

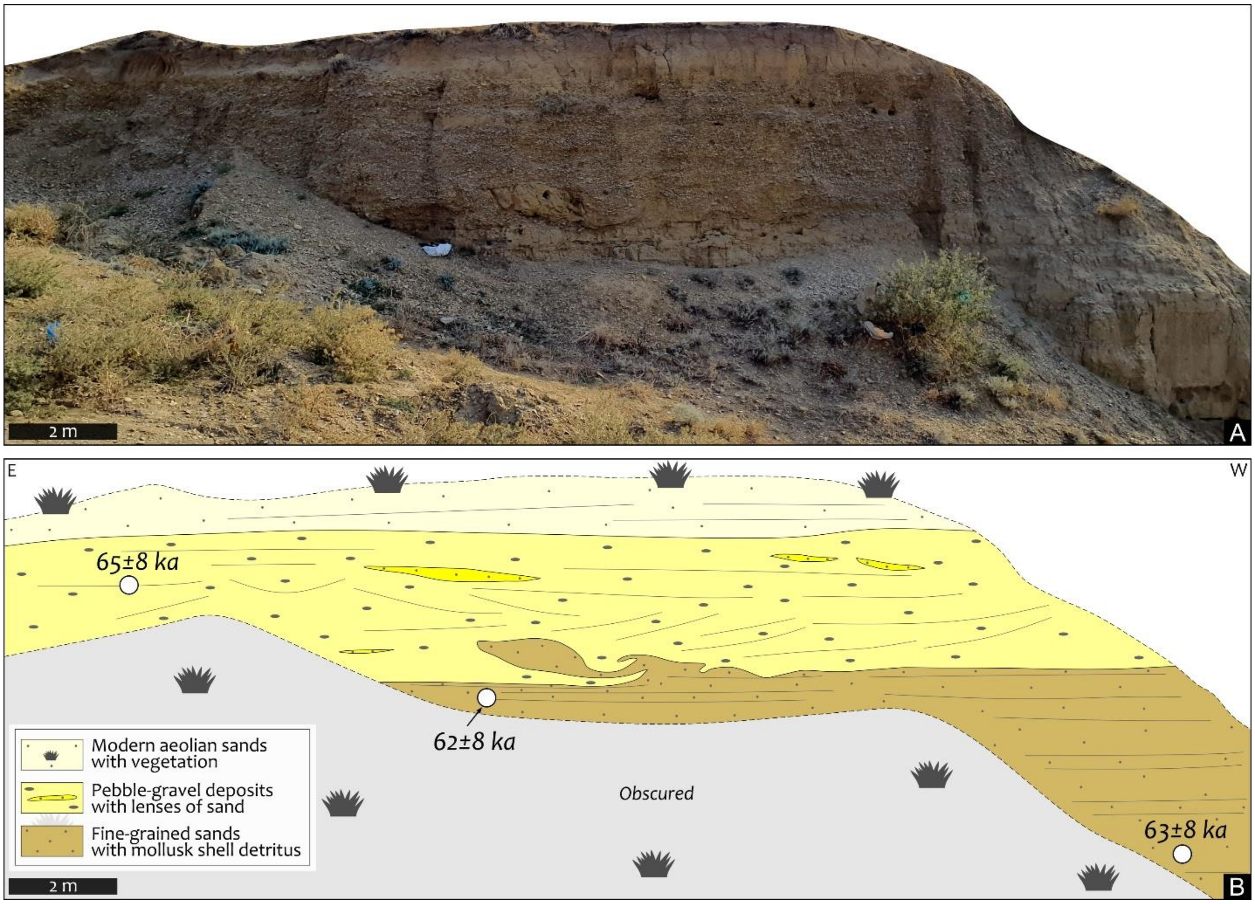

Figure 7. Outcrop on the right bank of the Shura-Ozen' River exposing substratum deposits of the Sarykum dune complex (SS): (A) general view of the site; (B) geological interpretation with quartz OSL ages of the main units. The location of the site is shown in Figures 3 and 4a.

4.1.2. Aeolian succession

4.1.2.1. Eastern quarry

The quarry is situated in the northwestern corner of the Eastern Sarykum (Figs. 3, 4). Its base lies at approximately 80-85 m a.s.l. Our study primarily focused on the N-NW facing wall in the northeastern part of the quarry (Fig. 8), where a 25-meter-thick aeolian succession was exposed (as of August 2022). The first 10 meters of the section (from the bottom), which we define here as lower aeolian unit (Fig. 6), consist of yellowish, primarily medium to coarse-grained quartz sands with layers of carbonate-cemented gravel to pebbles (up to 5 cm in size; Fig. 9b-c) and detrital of mollusk shells. These sands feature large planar cross-bedded series, reaching up to 2-3 meters in thickness (Fig. 9a). Within this interval, we obtained four quartz OSL-dates (Figs. 6, 8 and 9a; Table 1), with ages (from bottom to top) 68±6 ka (RGI-1105), 64±6 ka (RGI-1106), 53±6 ka (RGI-

1107), 69±5 ka (RGI-1108). The next 7 meters above are obscured by sand debris (Fig. 8); however, indistinct bedding planes of cemented gravel material (2-3 cm thick) are occasionally visible within this interval, resembling the cross-bedding pattern observed below (Fig. 9d-e).

Above this covered section, fine to medium grained quartz sands are exposed, forming the uppermost 5-7 meters of the section, which we define as upper aeolian unit (Figs. 6 and 9e). These sands do not exhibit clear cross-bedding but include at least four distinct subhorizontal layers of dark pedogenized sands enriched in organic matter, which serve as important stratigraphic markers distributed throughout the quarry. The thickness of the two lower pedogenized layers varies from 60-80 cm to just a few centimeters, while the upper two layers remain consistently thin, at about 10-12 cm in thickness (Fig. 9e). We collected three OSL samples within this interval: one from just 30 cm below the first pedogenized layer (layer ps-1), yielding a quartz age of 11.9±0.9 ka (RGI-1109); another from the second most pronounced pedogenized layer (Fig. 9e; ps-2), with a quartz age of 3.1±1.6 ka (RGI-1110); and a third sample (RGI-1111) 30 cm above the second pedogenized layer, for which paleodose and age were not obtained, as there was no natural luminescent signal from the quartz in the sample (Table 2).

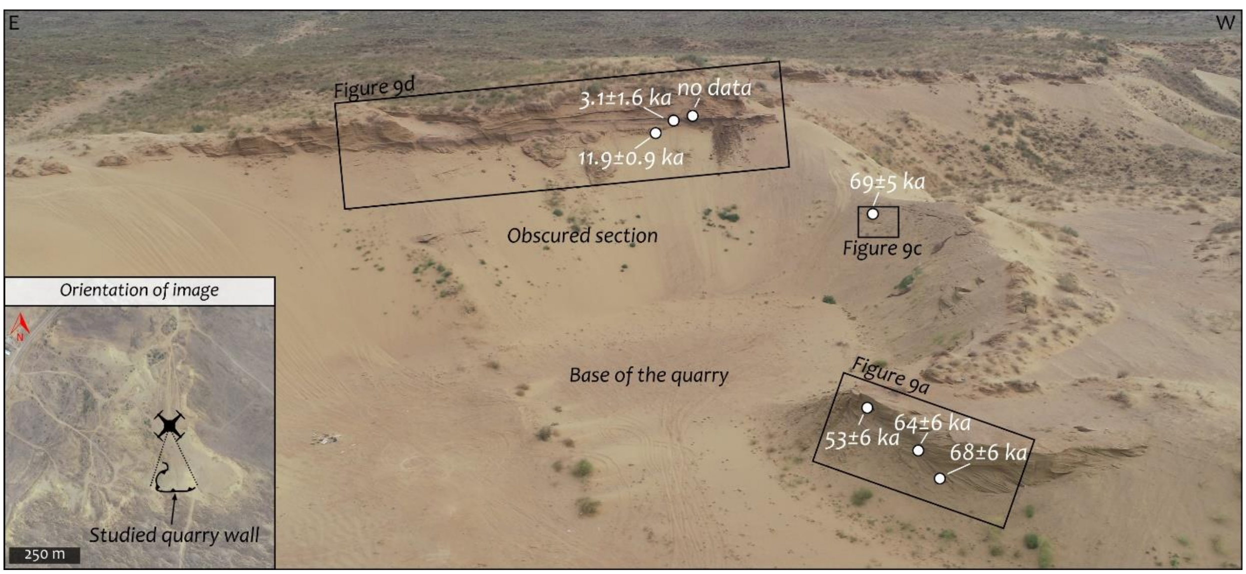

Figure 8. Drone view of the northeastern part of the quarry in the Eastern Sarykum (EQ) and main studied sections with quartz OSL ages. The orientation of the image is shown in the inset figure in the lower left corner. The location of the site is shown in Figures 3 and 4a.

Throughout the entire eastern quarry, we made 83 measurements of cross-bedding orientations within the lower aeolian unit, which features prominent cross-sets. These measurements indicate a dominant dip direction towards the NW and W, with minor dip directions towards the N and SW (Fig. 4a).

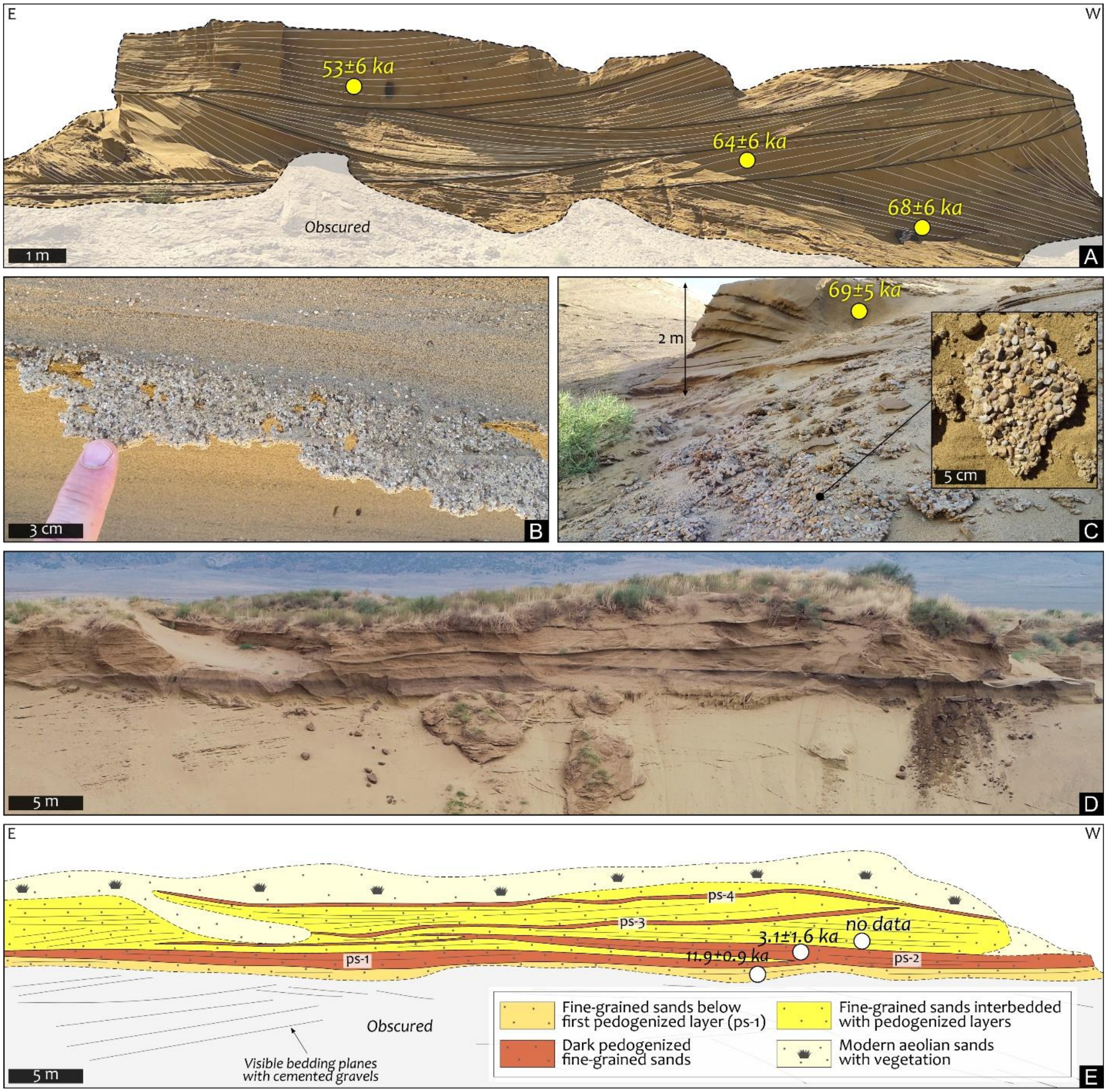

Figure 9. Main aeolian units and features of the eastern quarry (EQ): (A) lower aeolian unit with large cross-bedded series and obtained quartz OSL ages; (B) lenses of carbonate-cemented gravel in the lower aeolian unit; (C) layers with carbonate-cemented pebbles observed in the lower aeolian unit; (D) top of the section exposing the upper aeolian unit; (E) geological interpretation of the upper aeolian unit with quartz OSL ages; ps-1, ps-2, ps-3, ps-4 – layers with pedogenized sands. Details on the OSL data are given in Table 2. The location of the site is shown in Figures 3 and 4a.

4.1.2.2. Western quarry

The western quarry is situated in the western part of the Western Sarykum, 3.5 km NW of the Central Massif. This small, currently inactive quarry measures 190 by 85 meters, with its base lying at an altitude of approximately 105 m a.s.l.; however, it is uncertain whether this elevation corresponds to the base of the aeolian succession there.

The aeolian succession exposed in this quarry is similar to that observed in the Eastern Sarykum. The upper unit represents modern aeolian sands on top of the section and prominent layers of dark pedogenized sands below. The thickness of the upper unit here is about 8 meters. The lower unit consists of yellowish, predominantly medium to fine-grained sands (with a thickness up to 10 meters), characterized by planar cross-sets and subhorizontal layering. In the lower unit, there are regular layers and lenses of coarse-grained sands (up to 3 cm thick; Fig. 10a), and irregular lenses of gravel-pebble material with large, weakly rounded, and angular fragments (up to 40 cm in size) of sandstones (Fig. 10b). A total of 35 measurements of cross-bedding orientations were made in the lower unit, showing a dominant dip direction towards the SE (Fig. 4a). Due to strict time constraints, no OSL sampling was conducted in this quarry.

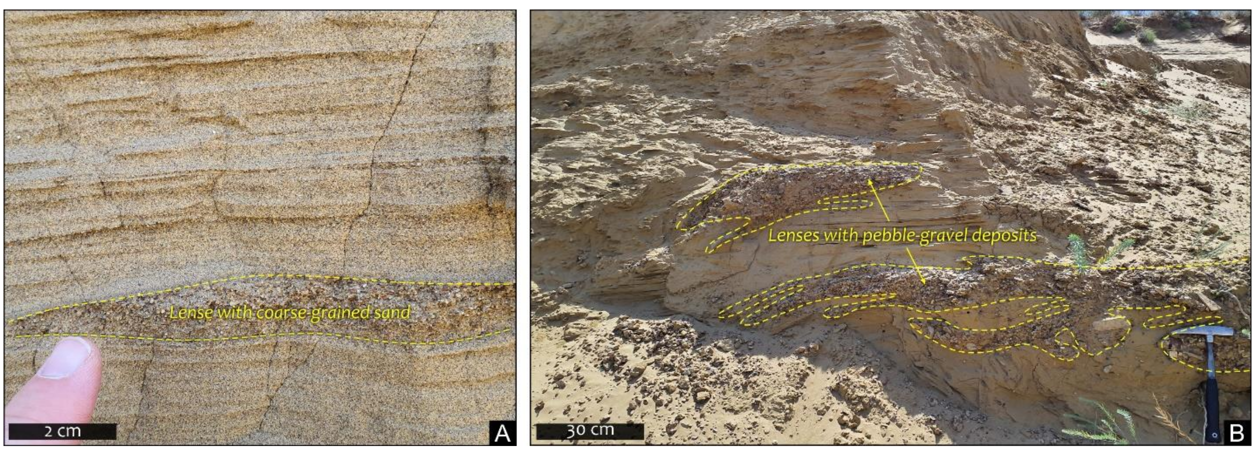

Figure 10. Main features of the lower aeolian unit exposed in the western quarry (WQ): (A) lenses with coarse-grained sand in the medium to fine-grained sands; (B) lenses with pebble-gravel material in the medium to fine-grained sands. The location of the site is shown in Figures 3 and 4a.

4.1.2.3. Blowout in the Central Massif

In the Central Massif, an old aeolian succession beneath the modern dune sands can be studied in a blowout located at an altitude of approximately 140 m a.s.l., which is 60-70 m above the base of the dune complex. This blowout is situated about 75 meters east of the northern tip of the largest active sand ridge and 75 meters north of the tourist viewpoint (Figs. 3, 4a, 5f, 11a).

The blowout exposed a 4-meter section (as of August 2022) of medium to coarse-grained yellowish quartz sands, characterized by planar cross-bedding and prominent carbonate cementation visible on the bedding planes and weathered surfaces (Fig. 11b, c). We obtained four OSL-dates from the sands (Fig. 11; Table 2), with quartz ages (from bottom to top) 7.9±0.6 ka (RGI-1112), 8.7±0.8 ka (RGI-1113), 8.1±0.6 ka (RGI-1114), 7.0±0.5 ka (RGI-1115). 77 measurements of cross-bedding orientations reveal a dominant dip direction towards SE, with minor dip directions towards the S and E (Fig. 4a).

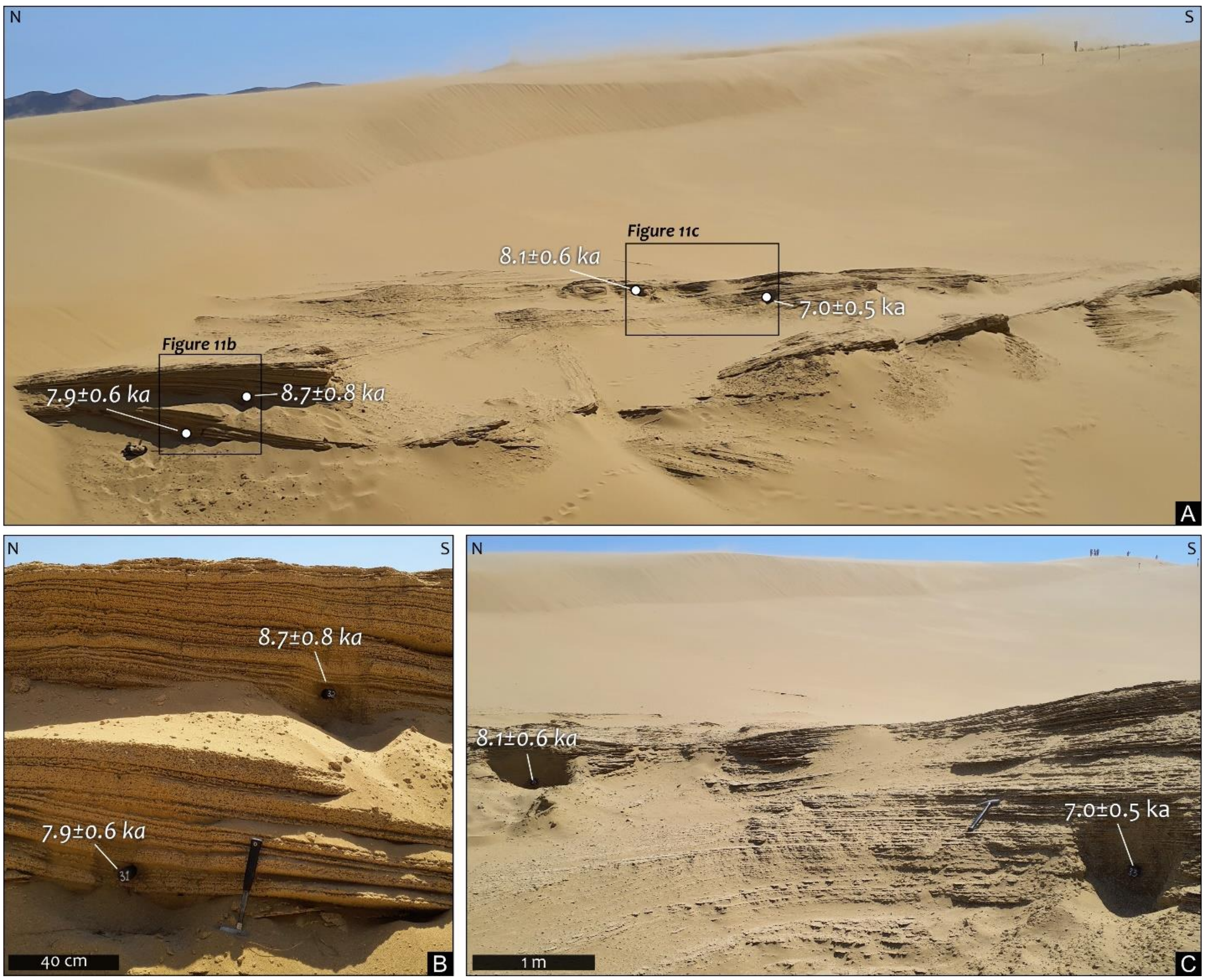

Figure 11. Blowout in the Central Massif: (A) – general view of the locality with the exposed carbonate-cemented coarse-grained sands featuring large planar cross-sets, along with the location of the OSL sampling sites (only quartz ages are shown); (B) lower part of the studied section; (C) upper part of the studied section. In the background of Figure 11A, note a wind storm affecting the dune crest and

transporting sand to the west-northwest (photo date: 27th August, 2022). Details on the OSL data are given in Table 2. The location of the site is shown in Figures 3 and 4a.

4.3. Modern wind data and aeolian sand drift potential

Strong winds exceeding 6.5 m/s in the Makhachkala region occurred during 13.5% of the recorded time, corresponding to 23187 measurements out of a total of 168959 observations for the 1966–2023 period (Fig. 12a). The prevailing directions of these strong winds align with the overall wind pattern, characterized by two opposing winds from SE and NW. The total drift potential (*DP*) value calculated from all wind measurements is 33.7 (based on wind velocities measured in m/s; Bullard, 1997), classifying the region overall as an intermediate-energy environment (Fig. 12b). Seasonal variations in *DP*, determined by analyzing monthly data across the full measurement period, indicate that February, with *DP* > 54, is characterized by a high-energy environment. In contrast, wind energy decreases during the summer months, with the May–September interval corresponding to a low-energy wind environment. The remaining months are characterized by an intermediate-energy environment. Notably, SE and NW winds dominate the energy balance, contributing over 80% of the total *DP* (Fig. 12b, 13a).

Despite lower *DP* values and the corresponding lower-energy environment compared to other months, the May–September interval exhibits intermediate directional variability in winds, as indicated by the *RDP/DP* ratios (Fig. 12c). During this period, either SE or NW winds dominate the wind rose (Fig. 12a). In contrast, the remaining months display higher directional variability, resulting in lower *RDP/DP* ratios (Fig. 12c). June–July and August–September show the highest and nearly equal *RDP* values among all months, with *RDD* oriented toward the SE and NW, respectively. However, the total *RDP* value for the entire year is low (2.2) due to the opposing directions of dominant resultant drifts in June–July and August–September. The total *RDD* is slightly oriented toward the NW, influenced by minor resultant drifts in the NW direction during October–November and April–May (Fig. 14a). Based on these characteristics, the wind regime near the Sarykum dune complex can currently be classified as obtuse bimodal, following the nomenclature of Fryberger and Dean (1979).

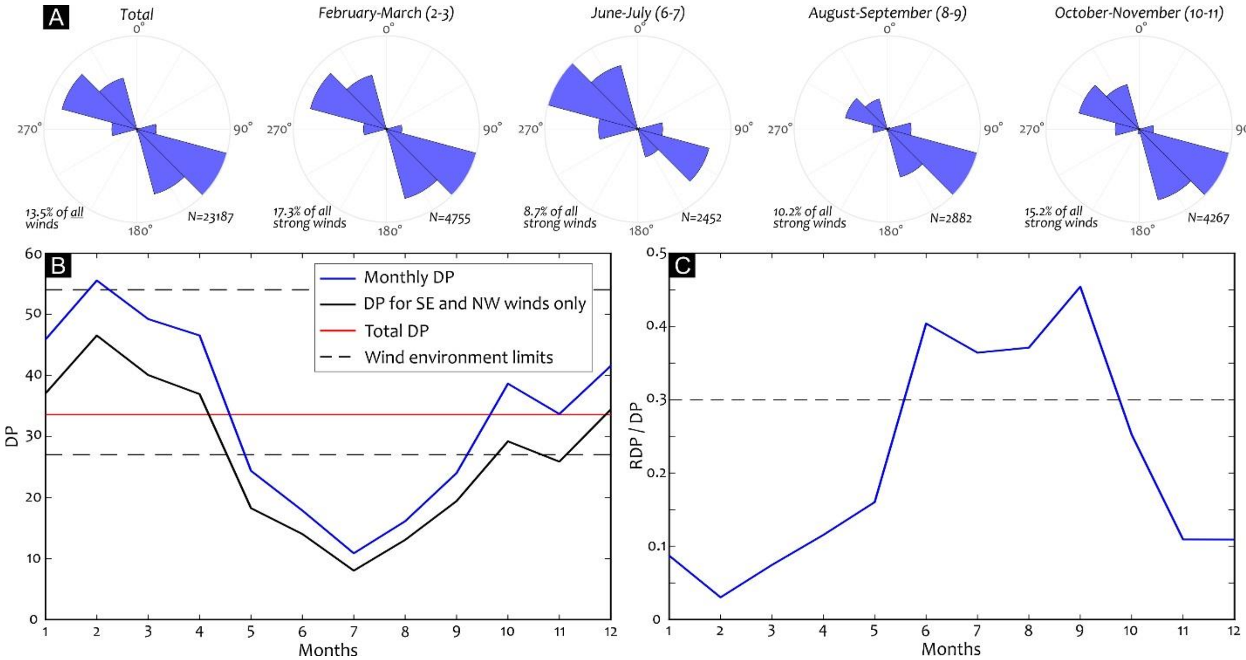

Figure 12. Monthly wind data analysis from the Makhachkala meteorological station (1966–2023): (A) Total and selected double-months wind roses for strong winds (>6.5 m/s). Number of used measurements, *N*, and the fraction of these measurements from all observations indicated in each panel. (B) Monthly *DP* variations, calculated by extracting data for each month over the entire measurement period. February *DP* > 54 indicates a high-energy environment, whereas May–September *DP* corresponds to a low-energy environment (dashed lines, after Bullard, 1997). The rest of the months are characterized by an intermediate-energy environment. The black line shows the dominance of SE and NW winds in the energy balance, accounting for more than 80% of total *DP*. This line is derived from winds directed within the intervals 105°–145° and 285°–325°. (C) Monthly variations in *RDP/DP* ratios, reflecting directional variability of the winds. The *RDP/DP* ratios are highest from May to September, indicating lower variability of wind directions.

The annual analysis of *DP* values reveals a noticeable decline in wind energy from 1966 to the present (Fig. 13a). During the 1966–1968 period, the region experienced a high-energy environment, with *DP* values exceeding 100. Subsequently, wind energy stabilized at intermediate levels between 1970 and 1984, with a notable high-energy peak in 1978. After 1986, the region transitioned to a low-energy wind environment, interrupted by two noticeable increases in *DP* values in 1994 and 1996. The *RDP* values during the observations varied drastically from the nearly zero values to 40-50, with only SE or NW resultant drift directions. A clear reduction in *RDP* values occurred after 1996 (Fig. 13b).

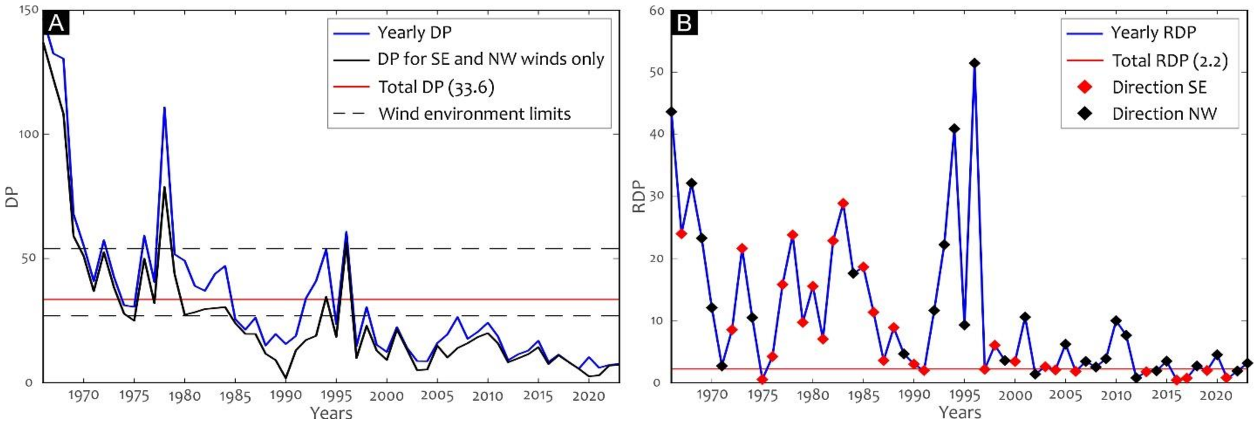

Figure 13. Annual wind data analysis of the from the Makhachkala meteorological station (1966–2023): (A) variations in *DP* values. Note a general decline in wind activity from 1966 to 2023. (B) B) Variations in *RDP*. Color-coded symbols indicate annual *RDD*s, which are only SE and NW.

To illustrate the potential sand drift over the observed period, we adopted the Fryberger and Dean (1979) assumption that sand drift is proportional to *DP*. The proportionality coefficient is uncertain and not explicitly defined due to complex interactions between wind and sand, as well as the potential temporal variability of this interaction. Thus, we assumed proportionality coefficient as one, allowing for an approximation of cumulative sand drift measured in units of *DP*.

Therefore, we represent the evolution of aeolian transport as the cumulative sum of the elementary drift potential vectors DP_j (eq. 1), starting at (0,0) in 1966 and progressing to 2023 at a location displaced toward the NW. The trajectory, shown in Figure 14b, reflects the net pattern of aeolian transport during the measurement period. This trajectory illustrates the meaning of drift potential measures, *RDP* and *DP*. The total *RDP* in Fig. 14a is calculated as the displacement vector between 1966 and 2023 (Fig. 14b) divided by the total number of measurements (eq. 3), while the length of the drift path (Fig. 14b) divided by the total number of measurements results in the total *DP* (eq. 2).

The cumulative drift pattern indicates a sand transport toward the NW from 1966 to 1971, followed by a shift toward the SE until 1992, and a subsequent return to NW-directed transport that persists to the present (Fig. 14b). It is important to note that the graph in Figure 14b simplifies the full complexity of aeolian transport dynamics, as much of the time *DP* alternates between SE and NW directions, often resulting in zero net displacement over shorter time intervals. The low total *RDP/DP* ratio (0.065) and monthly variations of *RDP* indicate that the sand drift is mainly SE-NW directions, leaving only a small portion to total displacement.

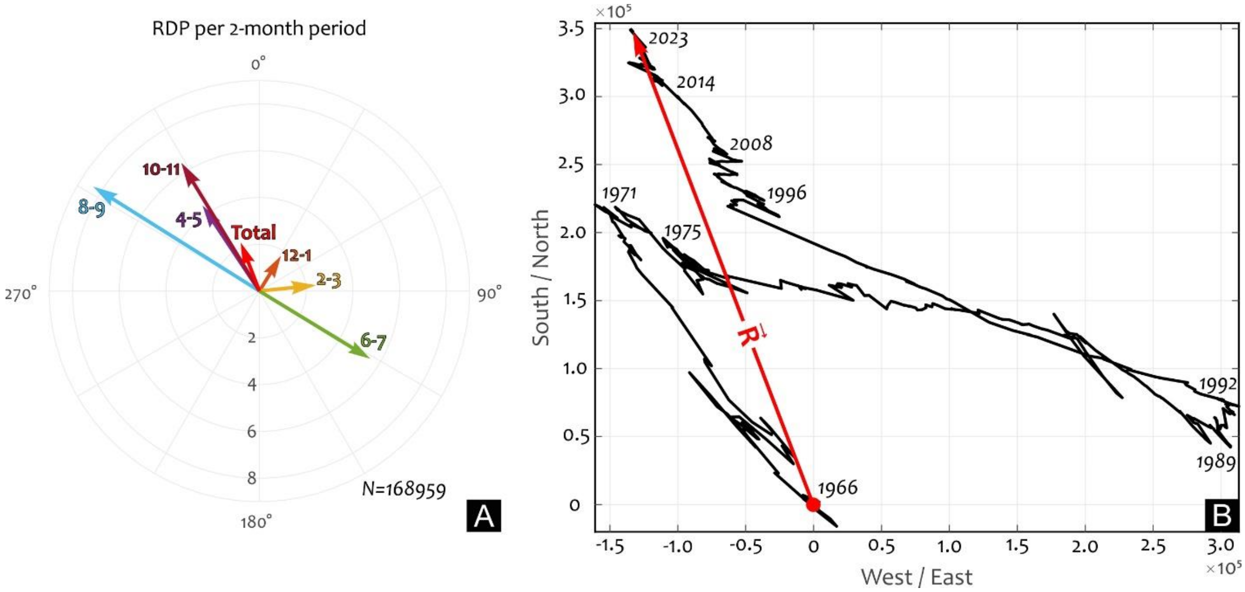

Figure 14. (A) Polar diagram of $\overrightarrow{RDP}$ for the 2 month periods (marked by months' numbers) and for all months together (marked by Total) for 1966-2023 period. *RDP* values are indicated along the 180° axis based on wind velocities measured in m/s. (B) Modelled relative sand drift path calculated for 1966-2023 period. Vector $\vec{R}\ \left(N \cdot \overrightarrow{RDP}\right)$ (see eq. 3) connects the first and the last points of measurements and approximates total displacement during drift.

5. Discussion

5.1. Phases of aeolian activity in the Sarykum dune complex and regional correlations

5.1.1. Onset of aeolian activity: Khazarian transgression and Atelian regression of the Caspian Sea

Understanding the stratigraphy and paleoenvironment that preceded the aeolian deposition is important for clarifying the chronology and key factors that governed the onset of aeolian activity in the region. The Sarykum dune complex is believed to be underlain by the deposits formed during the Khazarian transgression of the Caspian Sea (e.g., Fedorov, 1957; Rychagov, 1997), which provides a rough constraint for the maximum age of the dune complex as being post-Khazarian (e.g., Idrisov, 2010). However, many aspects regarding the stadiality, timing, and spatial extent of the Khazarian transgressive phase remain under debate (e.g., Fedorov, 1957, 1978;

Rychagov, 1997; Krijgsman et al., 2019; Zastrozhnov et al., 2024). Nonetheless, it is generally agreed that the Khazarian transgression occurred during MIS 10 to MIS 5. The peak of the transgression is believed to have happened during its earlier phase in the Middle Pleistocene, reaching a level of 20-35 m a.s.l. (e.g., Fedorov, 1978). The last phase of the Khazarian transgression likely occurred around 128-85 ka in the Late Pleistocene at MIS 5 (e.g., Krijgsman et al., 2019, and references therein; Zastrozhnov et al., 2020, 2021), with a sea level not exceeding 10 m b.s.l. (e.g., Yanina, 2014) (Fig. 15). The two phases of the Khazarian transgression are separated by the mild Singilian regression (Zastrozhnov et al., 2018), when the Caspian Sea level could drop down to 25 m b.s.l. (Fig. 15). The deposits of this phase have not yet been documented within the Sarykum dune complex area.

The Shura-Ozen' river valley near Sarykum is regarded as a stratotypical area for upper Khazarian deposits, distinguished by a characteristic assemblage of Caspian Didacna mollusks, as documented by Fedorov (1957). However the stratification of the terrace sequence still remain debatable. For instance, Fedorov (1957) interpreted thin lower Khazarian deposits resting on top of Sarmatian clays, however Rychagov (1997) questioned this interpretation, suggesting that these deposits belong to the upper Khazarian. Additionally, Rychagov (1997) interpreted the pebble-gravel deposits capping the terrace sequence (Figs. 6, 7) as late Khazarian alluvium, whereas Fedorov (1957) attributed them to post-Khazarian alluvial deposition. Both Fedorov (1957) and Rychagov (1997) agreed in defining the fine-grained sands with mollusk shell detritus (Figs. 6, 7), situated below the pebble-gravel layer, as late Khazarian marine sediments. This demonstrates that relying solely on malacological analysis of Caspian Sea sediments, without incorporating other geological methods, can result in conflicting stratigraphic interpretations. For example, Zastrozhnov et al. (2018, 2020, and 2021) showed that different researchers have considered the same deposits in the riverside outcrops in the Lower Volga region to be Bakunian, Singilian, lower Khazarian, or upper Khazarian.

The modern top level of the Khazarian deposits within the Sarykum dune complex is at an altitude of 70-80 m a.s.l. This suggests that the area has experienced significant uplift since the retreat of the Khazarian sea, with uplift magnitude exceeding 100 meters (e.g., Fedorov, 1957). Therefore, even a modest average uplift rate of 1 mm/year could be sufficient to raise the Khazarian sediments to their current altitude. This is plausible given that both the study area and the Caucasus region in general are tectonically active, known for significant seismicity and vertical neotectonic movements throughout the Quaternary and earlier epochs (e.g., Kaftan et al., 2024; Tatarinov et al., 2024). Notably, the 1970 Dagestan earthquake (M=6.6) had its epicenter near the Sarykum dune complex within the Narat-Tyube Ridge (Lukk and Sidorin, 2022, and references therein).

The Atelian regression, which succeeded the Khazarian transgression, was marked by a drastic decrease in the Caspian Sea level at around 80-30 ka during MIS 4 and MIS 3 (Fig. 15) (e.g., Eremin and Molostovsky, 1981; Eremin, 1986; Shakhovets, 1987; Bezrodnykh et al., 2015; Taratunina et al., 2021, 2022; Kurbanov et al., 2022). According to various estimates, the sea level dropped to 70÷100 m b.s.l. (Bezrodnykh et al., 2004, 2015), or even down to 140 m b.s.l. (Lokhin and Maev, 1990). However, some studies (e.g., Badyukova, 2021) question the existence of a significant regressive phase at that time. This period was characterized by cold and arid climatic conditions associated with the early Valdai (Weichselian) glacial epoch, leading to increased dust accumulation, vegetation degradation, and substrate drying. These factors contributed to the formation of loess-like deposits across large areas of the Caspian Depression and its surroundings.

Our OSL results indicate that the alluvial deposits capping the terrace were formed around 65 ka (Figs. 6, 7; Table 2), confirming their deposition at the onset of the Atelian regression, thereby supporting the age interpretation proposed for these deposits by Fedorov (1957). The fine-grained sands with mollusk shell detritus beneath the alluvial pebble-gravel layer yielded similar OSL ages of 63–62 ka (Figs. 6, 7, 15; Table 2), further correlating with the Atelian phase. Finally, OSL dating of the lower aeolian unit of the Sarykum dune complex, which is exposed in the eastern quarry (Figs. 6, 8, 9a; Table 2), produced ages ranging from 69 to 53 ka, also aligning these sediments with the arid Atelian phase. Although the aeolian succession in the western quarry was not sampled, the similarity between the eastern and western sections suggests they may have formed under similar conditions and within the same timeframe. Further dating of the western quarry is needed to confirm this. It is also intriguing to consider a potential correlation between the formation of the Sarykum sands and thick loess-like deposits found in the Khasavyurt district, located 60 km northwest of the dune complex (Fig. 1b). These deposits bear similarities to typical Atelian loesses exposed along the Lower Volga region, although, currently, there is no absolute chronology available for them (Idrisov, 2011, 2014).

The similar ages of the lower aeolian unit at the Eastern Sarykum and the underlying alluvial pebble-gravel deposits suggest that the development of the Shura-Ozen’ River valley began with the onset of aeolian activity, driven by the aridification of the climate during the Atelian regression (Fig. 15). Evidence of aeolian-fluvial interaction is also exemplified by coarse-grained layers and lenses in the lower aeolian sands found in both the eastern and western parts of the Sarykum dune complex (Figs 9b, 9c, 10a, 10b). The Atelian ages obtained for the fine-grained sands beneath the alluvial deposits (Figs. 6, 7), previously interpreted as marine (Fedorov, 1957; Rychagov, 1997), suggest two possibilities: (1) a marine environment may have persisted in the area until 70–60 ka, or (2) the existing lithogenetic and biostratigraphic interpretations require revision, potentially linking this sandy layer to the onset of aeolian activity following the retreat of the Khazarian sea. Additionally, based on the grain size of the sand matrix in both the alluvial deposits of the supposed high river terraces and the aeolian sands of the Sarykum dune complex, Gusarov (2018) suggested that the accumulation of Sarykum sands could begin even before the incision of the Shura-Ozen' valley. However, the alluvial complexes and associated terraces of the Shura-Ozen' River remain poorly understood and require further detailed studies.

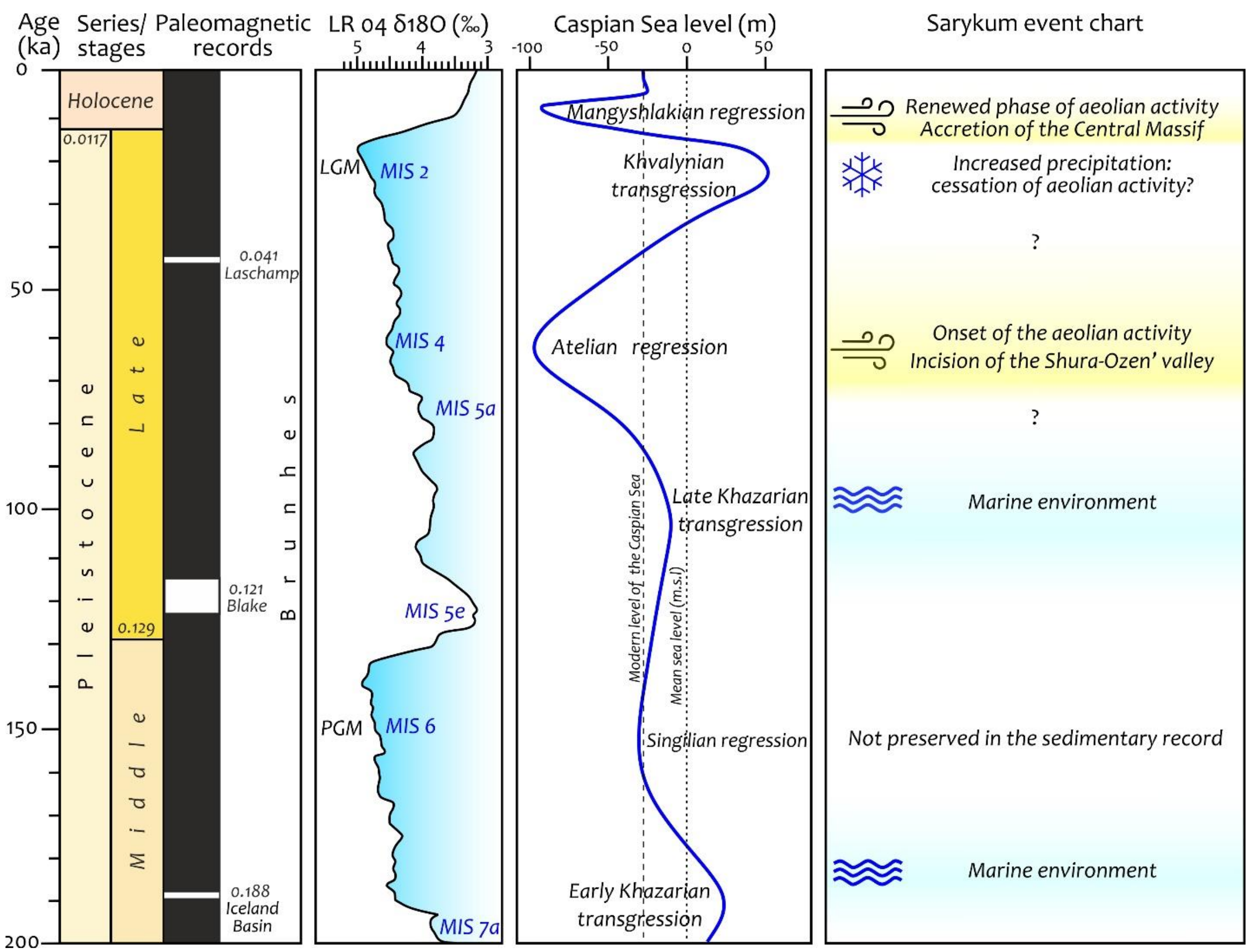

Figure 15. Event summary for the Sarykum dune complex. The chronostratigraphic chart, paleomagnetic records, marine isotope stages (MIS), and oxygen isotope fractionation are from Gibbard and Cohen (2019). Caspian Sea level variations are based on literature data (see text for details). LGM – Late Glacial Maximum, PGM - Penultimate Glacial Period.

Paleowind directions inferred from cross-bedding orientations in the lower aeolian unit of the Eastern Sarykum indicate prevailing winds blowing toward the NW during the period of their deposition in the Atelian phase (Fig. 4a). In contrast, cross-bedding of the lower unit within the Western Sarykum indicates an opposite paleowind direction (Fig. 4a). If the lower aeolian unit in the western quarry are contemporaneous with that in the eastern quarry, these opposing paleowind directions might reflect seasonal shifts in paleowind regimes. This interpretation aligns with the modern wind regime, characterized by strong bimodal winds capable of transporting sand. The highest cumulative drift potential occurs in June–July and August–September, with winds predominantly blowing toward the southeast and northwest, respectively (Figs. 12c and 14a).

5.1.2. Khvalynian transgression and Mangyshlak regression: cessation and subsequent renewal of aeolian activity

After the Atelian regressive stage, the Caspian Sea underwent a significant transgressive episode known as the Khvalynian transgression, during which the sea level rose to approximately 50 m a.s.l. (Fig. 15) (e.g., Fedorov, 1957; Svitoch, 2007). However, this transgression did not reach the area of the Sarykum dune complex. In fact, the Khvalynian transgression is believed to have occurred around 30-12 ka (e.g., Bezrodnykh et al., 2004, 2015; Kurbanov et al., 2021, 2022); albeit, the magnitude and stadiality of this event remain subjects of ongoing debate (e.g., Makshaev and Tkach, 2022; Zastrozhnov et al., 2024). Recent OSL data suggest that the maximum extent of the Khvalynian sea occurred around 20-15 ka, coinciding with the Late Glacial Maximum (LGM) (Taratunina et al., 2022, 2024), and was likely driven by increased runoff from the Volga River. Palynological records from Khvalynian sediments in the Lower Volga region indicate periglacial landscapes and harsh climatic conditions during this time (e.g., Bolikhovskaya and Makshaev, 2020). Data from caves in the North Caucasus suggest that the region experienced a warmer climate around 29-25 ka, followed by severe cold conditions and perhaps persistent snow cover during the LGM (e.g., Golovanova et al., 2021). Notably, aeolian sediments corresponding to the

Khvalynian stage have not been documented within the Sarykum dune complex. This absence could be due to the later removal and reworking of these deposits during the following phases or a temporary break in aeolian activity during the Khvalynian transgression, possibly caused by increased precipitation.

Our results indicate that the Pleistocene-Holocene transition appears to have marked a significant period of aeolian activity in the study area. This is evidenced by OSL dating of the sand layer just beneath pedogenized sands in the upper aeolian unit of the eastern quarry (Figs. 6 and 9e), suggesting that aeolian reactivation may have begun as early as 13-11 ka. This aeolian phase could continue until at least 8-7 ka, as inferred from the OSL dating of the sediments studied in the blowout in the Central Massif. However, the overall chronology of the Central Massif's development remains uncertain, primarily due to the limited exposures, which restrict detailed study from its base to summit. Despite these limitations, our results indicate that by the early Holocene, the Central Massif had reached a height of at least 70 meters from its base, approximately half of its current elevation. It is also plausible that by this time, the massif had already attained a height closer to its present elevation, with the studied sediments potentially being redeposited near the flanks of previously accreted dune ridges.

This renewed aeolian activity coincides with the Mangyshlak regression, a period when the Caspian Sea level dropped to 70÷90 m b.s.l. (Fig. 15) (e.g., Bezrodnykh et al., 2004; Maev, 2009). While the precise timing of this lowstand event remains debated, it is generally estimated to have occurred between 12.5 and 7 ka (e.g., Bezrodnykh et al., 2004; Richards et al., 2014; Bezrodnykh and Sorokin, 2016). The palynological records from the North Caspian region (e.g., Richards et al., 2014) and mountainous Dagestan (e.g., Ryabogina et al., 2019) indicate dry climate with warm and cold episodes at that time with activation of wind-blown processes. The formation of the enigmatic Baer Knolls, linear accumulative ridges that span vast areas of the Caspian Depression, was also attributed to aeolian activity during the Mangyshlak regression (e.g., Volkov, 1960; Kroonenberg et al., 1997; Richards et al., 2014). Notably, the OSL dates from the Central Massif correlate well with the '8200-year cold event' (Alley et al., 1997), a short-lived global climatic shift characterized by dry and cold conditions and increased wind activity.

The paleowind analysis of the sediments in the Central Massif suggests that they were formed under predominantly SE-blowing paleowinds during their accumulation in the early Holocene (Fig. 4a). This reconstructed paleowind direction is similar to that observed in the lower aeolian sands of the western quarry and aligns with the modern wind regime, where strong SE-blowing winds with high cumulative drift potential are typical for June and July (Fig. 14a).

5.1.3. Post-Mangyshlak phase and recent development

By the end of the Mangyshlak phase, the development of the Sarykum dune complex was largely complete, and aeolian activity in the study area began to slow down. This reduction in activity was likely influenced by increased vegetation, as evidenced by the presence of pedogenized layers observed in the upper aeolian units in both the Western and Eastern Sarykum (Fig. 9e) and changes in adjacent lowland areas (Ryabogina et al., 2022). The OSL date from the lower pedogenized layer in the eastern quarry aligns well with the previous radiocarbon dates from the pedogenized sandy layers of 3.5 ka, 2.2 ka, and 1.9 ka (Idrisov, 2010; Gusarov, 2016), which were the only geochronological data available for the Sarykum dune complex prior to this study.

Presently, the development of the dune complex is largely influenced by vegetation, which controls the stabilization and periodic reactivation of blowouts, reshaping pre-existing topography of the Western and Eastern Sarykum. These blowouts are elongated in NW-SE direction, with depositional lobes forming at both ends, indicating that sediment transport is generally aligned with present-day wind regime. In the large blowouts in the western part of the dune complex, partly vegetated depositional lobes, which have progressed into sand sheets, are mainly developed on the SE sides (Fig. 5d). Given that the current wind regime produces a relatively low resultant drift trending toward the NW (Fig. 14), this implies that the wind regime in the recent past may have been slightly different, with the primary sand drift direction oriented toward the SE. The multidecadal changes in hydrometeorological parameters including the wind regime across the Caspian region over the past 70 years have been extensively documented (e.g., Gusarov, 2016; Kostianoy et al., 2019; Vyruchalkina et al., 2020; Kazmin, 2021; Gontovaya et al., 2023). These regional trends align with the patterns observed in our study, highlighting a significant decline in wind activity, transitioning from a high-energy to a low-energy environment (Figs. 13a, 14b). According to Vyruchalkina et al. (2020), during the 1948–2017 interval, periods of Caspian Sea level drop were characterized by dominant winds from the east that transported dry and warm air masses from Central Asia, thereby enhancing evaporation from the Caspian Sea. Conversely, during periods of sea level rise, northerly winds prevailed, reducing evaporation rates and contributing to water level increases.

The opposing nature of the strong winds also controls overall spatial stability of the large active dune ridges within the Central Massif (e.g., Gusarov et al., 2016; Balykova and Andreeva, 2023). These ridges migrate over short distances during both SE and NW wind events. The southeastern slope of the Central Massif has been modified by a network of climbing dunes (Fig. 5f). Gusarov (2015) and Gusarov et al. (2016), referencing Maiorov (1927), noted the existence of a sand quarry that was active in the early twentieth century which allegedly destroyed a significant portion of the southeastern slope. The suggested location of this quarry overlaps with the area where climbing dunes are present, leading Gusarov (2015) and Gusarov et al. (2016) to conclude that the morphology of the southeastern slope was shaped by slope processes initiated by human activity. However, our review of Maiorov's original publication (1927), which documents his extensive fieldwork in the Sarykum dune complex between 1915 and 1926, does not corroborate the existence of such a quarry. Instead, Maiorov (1927) describes a system of ridges on the southern slope of the Central Massif that are perpendicular to the main ridges. These ridges are depicted in a photo illustration included in his work as supplementary material, and they undoubtedly represent the climbing dunes, which we observe today. Therefore, we assert that these climbing dunes are of natural origin and are not linked to anthropogenic impacts and slope processes. The morphology of the climbing dunes indicates that winds from S-SW were responsible for their formation. These winds, which run nearly parallel to the Shura-Ozen' valley, likely originate as minor wind currents from the Narat-Tyube Ridge or from the deflection of more dominant winds influenced by the surrounding topography.

5.2. On the origin of the dune complex and the proposed model for its development

Perhaps, except for the provenance of sand material, attributed to the Middle Miocene quartz sandstones of the Narat-Tyube Ridge (e.g., Maiorov, 1927; Idrisov, 2010; Matsapulin et al., 2013; Gusarov, 2016), other key aspects of the evolution of the Sarykum dune complex remain unclear. These include the isolated nature of the complex, situated far from other large dune fields; the large volume of sediments concentrated in a relatively small area; the topographic influence facilitating this concentration; and the drivers responsible for sediment transport prior to aeolian redeposition (e.g., Gusarov, 2016). Our results indicate that aeolian deposition in the area began immediately after the retreat of the Khazarian sea (Fig. 15). Given the local source and long-lasting aeolian deposition supported by frequent strong winds, the concentration of aeolian material here must be explained by specific local features that promoted the accumulation of sands and vertical build-up of the dune complex.

Gusarov (2015, 2016) emphasized the role of the Shura-Ozen’ River in concentrating sand material. He proposed that the Sarykum sand material, before undergoing partial aeolian reworking, initially originated as deposits from the Shura-Ozen fluvio-deltaic basin, which developed on the abandoned marine plain of the Caspian Sea. He suggested that the sands with coarse-grained lenses in the Western and Eastern Sarykum, along with the sediments exposed in the Central Massif blowout, are remnants of this deltaic system. These deposits, intermixed with alluvial fans from the surrounding mountains, collectively form the core of the dune complex. This conclusion seems unrealistic for us, as it fails to explain how the proposed fluvio-deltaic basin could have formed so close to the mountain front, which at that time should have been bordered by the sea. There was no accommodation space for such a deltaic system to account for the thick and isolated deposits supposedly observed at high elevations within the Central Massif, given that the alluvial plain was too narrow and the sea basin too shallow. This scenario becomes even more problematic under the assumption that river incision began after aeolian deposition. In such a case, the required incision rates would exceed observed rates, conflicting with the valley and marine terrace morphology. Furthermore, the dip directions of the studied sediments indicate sediment transport perpendicular to the Shura-Ozen’ valley, aligning with the prevailing modern wind regime. This evidence strongly suggests an aeolian, rather than fluvial, origin for these deposits.

It is clear that the Shura-Ozen’ River played a role in sediment supply to the Sarykum aeolian system; however, within the study area, it typically deposits coarse-grained material such as gravel and pebbles, rather than sand. Given the limited sand supply from the Shura-Ozen' River, the relatively narrow floodplain, and the vast scale of the Sarykum dune complex, it is highly unlikely that it can be classified as a source-bordering, riverine foredune system.

We propose that landscape and drainage dynamics, as well as the regional wind regime were critical in the formation and growth of the dune complex. During the Khazarian transgression, when the Caspian Sea approached the mountain front, clastic material from the Shura-Ozen’ River and alluvial fans sourced from the uplifting Narat-Tyube Ridge fed into the sea basin. Additional material could have been contributed through wind abrasion of the highlands. These sediments were likely sorted in the beach and littoral zones. After the Caspian Sea retreated during the Atelian phase, they became susceptible to aeolian reworking across the abandoned marine plain, which extended along the mountain front from the Kizilyurt district in the west to the Makhachkala region in the east (Fig. 1b). Concurrently, the Shura-Ozen' River began incising into the abandoned marine plain, interacting with the developing aeolian system. This fluvial-aeolian interaction is evidenced by the layers and lenses of pebbles and gravel within the aeolian succession. Idrisov (2010) and Gusarov (2015) noted the absence of paleontological evidence, such as fragments of Caspian mollusk shells, within the Sarykum sands, casting doubt on the idea that these sands were sourced from marine coastal deposits. However, our observations show that shell detritus is relatively abundant within the sands. Therefore, it is plausible that the disintegration or even pulverization of shell fragments prior to burial occurred over sufficient time for mechanical breakdown during aeolian transport and reworking.

Our analysis indicates that the reversing NW-SE winds, which blow subparallel to the Narat-Tyube Ridge, could persist in the area for at least 70 000 years, since the Atelian phase. These winds played a crucial role in sediment transport and the development of the Sarykum dune complex. It is likely, based on current observations, that the sand material was supplied from both the NW and SE directions, with a stronger tendency for supply from the NW. As the incision of the Shura-Ozen' valley progressed, fluvial processes became increasingly dominant, affecting the aeolian sediment transport capacity and ultimately hampering the progression of the sand material, trapping and accumulating it on the river banks. The presence of larger and thicker dunes on the left NW bank of the Shura-Ozen' River further supports the idea of dominant sediment supply from NW. The relative spatial stability and growth of the dune complex throughout its evolution were largely influenced by intermittent periods of increased vegetation and precipitation, along with the reversing patterns of the regional winds.

6. Conclusions

This study provides, for the first time, insights into the chronology of the Sarykum dune complex's evolution. The dune complex began to develop approximately 70 ka during the Atelian phase, when the Caspian Sea experienced significant regression, caused by a drier climate that facilitated the regional accumulation of wind-blown sediments across large areas of the North Caspian region. Aeolian activity likely ceased during the Khvalynian phase (30-12 ka), characterized by a rise in the Caspian Sea of up to 50 m a.s.l, with specific climate conditions associated with the LGM inhibiting aeolian processes.

A renewed phase of aeolian activity began at the Pleistocene-Holocene transition, associated with another lowstand episode of the Caspian Sea known as the Mangyshlak regression, which occurred approximately 12.5-7 ka. Following the Mangyshlak phase, aeolian activity decreased, becoming intermittent and increasingly influenced by vegetation; this ultimately led to the stabilization of most of the dune complex, except for the dune ridges within the Central Massif.

The reversing NW and SE winds, currently dominant in the study area, persisted during the Late Pleistocene-Holocene and played a pivotal role in aeolian sediment transport and redeposition. Along with intermittent periods of increased vegetation and precipitation, these factors supported the relative spatial stability of the dune complex. The development of the dune complex has been closely tied to the Shura-Ozen’ River since its inception. The river cuts through the dune complex, shaping its morphology by serving as a topographic barrier that traps sediments, which accumulate primarily along its banks. The stronger tendency for sediment supply from the NW may explain the greater accretion of aeolian landforms on the left NW bank of the river compared to the right SE bank. By the early Holocene, the large aeolian Central Massif on the left bank of the Shura-Ozen’ River had already emerged as the dominant topographic feature within the dune complex, having accreted to at least half of its current elevation.

Our findings highlight that regional climate aridization, which drove fluctuations in Caspian Sea levels, was one of the key factors in reshaping paleo-landscapes in the North Caspian region, as demonstrated by the formation of the Sarykum dune complex. Further investigation into the development of the dune complex, including geochronological and biolithostratigraphic studies of its aeolian succession; substratum deposits; the incision history of the Shura-Ozen’ River; and neotectonic uplift in the study area and surrounding mountains, clearly merits additional research. These studies will help to refine our understanding of past climatic events and model future developments of the Caspian Sea.

Acknowledgments

The fieldwork was financially supported by the assignment from Rosnedra No. 049-00016-21-00 on conducting work on composite and overview mapping of the Russian Federation in 2020-2022. We extend our gratitude to the administration and staff of the Dagestan Nature Reserve for granting permission and providing assistance during fieldwork and drone surveys within the Sarykum dune complex. We also sincerely thank Simon Buckley for providing an academic license for Lime software (https://www.fonixgeo.com/lime/). Editing support from Lucy Medvedeva is greatly appreciated.

References

Agisoft (2022). Agisoft Metashape User Manual: Professional Edition, Version 1.8. Agisoft LLC, St. Petersburg, Russia, p. 212.

Alley, R. B., Mayewski, P. A., Sowers, T., Stuiver, M., Taylor, K. C., & Clark, P. U. (1997). Holocene climatic instability: A prominent, widespread event 8200 yr ago. Geology, 25(6), 483-486.

Badyukova, E. N. (2021). Caspian Sea level fluctuations in the Neopleistocene (was there an Atelian regression?). Oceanology, 61(2), 283-291.

Bagnold, R.A. (1941). The physics of blown sand and desert dunes. London, Chapman & Hall, 265 p.

Balykova, S., & Andreeva, T. (2023). Dune Massifs of Russia. In Sand Dunes of the Northern Hemisphere: Distribution, Formation, Migration and Management (pp. 181-201). CRC Press.

Barbot de Marny, N.N. (1894). Otchet o geologicheskikh issledovaniyakh v Termirkhan-Shurinskom okruge Dagestanskoi oblasti [A report on the geological investigations in the Temirkhan-Shura district of the Dagestan region]. Materials on the geology of the Caucasus, 2, 8, 228-409. In Russian.

Barchyn, T. E., & Hugenholtz, C. H. (2013). Reactivation of supply-limited dune fields from blowouts: A conceptual framework for state characterization. Geomorphology, 201, 172-182.

Bezrodnykh, Y. P., Romanyuk, B. F., Deliya, S. V., Magomedov, R. D., Sorokin, V. M., Parunin, O. B., & Babak, E. V. (2004). Biostratigraphy and structure of the Upper Quaternary deposits and some paleogeographic features of the north Caspian region. Stratigr. Geol. Correl, 12(1), 102-111.

Bezrodnykh, Y. P., Sorokin, V. M., Yanina, T.A. (2015). Ob atel’skoi regressii Kaspiiskogo moray [About the Atelian regression of the Caspian Sea]. Vestnik Moskovskogo Universiteta. Seria 5 Geografia, 2, 77-85. In Russian.

Bezrodnykh, Y. P., & Sorokin, V. M. (2016). On the age of the Mangyshlakian deposits of the northern Caspian Sea. Quaternary Research, 85(2), 245-254.

Bolikhovskaya, N. S., & Makshaev, R. R. (2020). The Early Khvalynian stage in the Caspian Sea evolution: pollen records, palynofloras and reconstructions of paleoenvironments. Quaternary International, 540, 10-21.

Buckley, S. J., Ringdal, K., Naumann, N., Dolva, B., Kurz, T. H., Howell, J. A., & Dewez, T. J. (2019). LIME: Software for 3-D visualization, interpretation, and communication of virtual geoscience models. Geosphere, 15(1), 222-235.

Bullard, J. E. (1997). A note on the use of the" Fryberger method" for evaluating potential sand transport by wind. Journal of Sedimentary Research, 67(3), 499-501.

Bulygina, O.N., Veselov, V.M., Razuvaev, V.N., Aleksandrova, T.M. (2014). Opisaniye massiva srochnykh dannykh ob osnovnykh meteorologicheskikh parametrakh na stantsiyakh Rossii [Description of an array of urgent data on the main meteorological parameters at Russian stations]. Certificate of state registration of the database No. 2014620549. http://aisori-m.meteo.ru/waisori/index.xhtml?idata=19 (date of access: 31/05/2024). In Russian.

Cohen, K. M., & Gibbard, P. L. (2019). Global chronostratigraphical correlation table for the last 2.7 million years, version 2019 QI-500. Quaternary International, 500, 20-31.

Enna, N.L., Lavrischev, V.A., Shishov, V.S., Pismenny, A.N., Aseeva, O.E., Pismenskaya, G.A. Gosudarstvennaya geologicheskaya karta Rossiiskoi Federatsii. Masshtab 1:200 000. Izdaniye vtoroye. Seriya Kavkazskaya. List K-38-XII (Makhachkala) [State geological map of the Russian Federation. Scale 1:200 000. Second generation. Caucasus series. K-38-XII (Makhachkala) map sheet]. VSEGEI, 211 pp. In Russian. In press.

Eremin, V.N. (1986). Stratigraphiya noveishykh otlozheniy Nizhnego i Srednego Povolzhya po paleomagnitnym dannym [Stratigraphy of the recent deposists of the Lower and Middle Volga regions based on paleomagnetic data]. PhD thesis, Moscow State University. In Russian.

Eremin, V.N., Molostovsky, E.A. (1981). Paleomagnitnyy razrez pleystotsena Nizhnego Povolzh'ya [Paleomagnetic section of the Pleistocene of the Lower Volga region]. Bulletin of the Academy of Sciences of the USSR, Geological series, 7, 71–76. In Russian.

Fedorov, P.V. (1957). Stratigrafiya Chetvertichnykh Otlozheniy i Istoriya Razvitiya Kaspiyskogo Morya [Stratigraphy of the Quaternary Sediments and the History of the Caspian Sea Development]. Proceedings of the Geological Institute of the USSR Academy of Sciences; Iss. 10, , Moscow, p. 298. In Russian.

Fedorov, P.V. (1978). Pleistotsen Ponto-Kaspiya [The Pleistocene of the Ponto-Caspian Region]. Nauka Press, Moscow, p. 165. In Russian.

Fryberger, S.G., Dean, G. (1979). Dune forms and wind regime (No. 1052), A study of global sand seas. United States Geological Survey.

Golovanova, L. V., Doronicheva, E. V., Doronichev, V. B., Tselmovich, V. A., & Shirobokov, I. G. (2021). Impact of climatic stresses and volcanism on the tendencies of the cultural process in the North Caucasus during the late Pleistocene. Izvestiya, Atmospheric and Oceanic Physics, 57(7), 781-802.

Gontovaya, I. V., Gavrilova, E. V., Tatarnikov, V. O., & Ocheretnyi, M. A. (2023). Long-term Changes in the Wind Regime in the Northwestern Caspian Sea. Russian Meteorology and Hydrology, 48(11), 1005-1010.

Guérin, G., Mercier, N., Nathan, R., Adamiec, G., & Lefrais, Y. (2012). On the use of the infinite matrix assumption and associated concepts: a critical review. Radiation Measurements, 47(9), 778-785.

Gusarov, A. V. (2014). Granulometricheskiy i mineralnyi sostavy peskov eolovo-akkumulyativnogo kompleksa “Sarykum” [Granulometric and mineral composition of sands from aeolian-accumulative complex “Sarykum”]. Proceedings of the state nature reserve “Dagestanskiy”, Makhachkala, 9, 28-39. In Russian.

Gusarov, A. V. (2015). Eolovo-akkumulyativnyi kompleks «Sarykum» kak unikalnyi geomorphologicheskiy ob’yekt Rossi: istoriya izucheniya i gipotezy proiskhozhdeniya [Aeolian-accummulative complex «Sarykum» as unique geomorphological object in Russia: research history and hypotheses of origin]. Geomorfologiya, 2, 54-71. In Russian.

Gusarov, A. V. (2016). Eolovo-akkumulyativnyi kompleks « Sarykum » - unikalnyi geomorphologicheskiy ob’yekt Rossi: stroeniye, genezis, istochniky peskov [Aeolian-accummulative complex « Sarykum » - unique geomorphological object in Russia: structure, genesis, sand sources]. Geomorfologiya, 3, 52-78. In Russian.

Gusarov, A. V., Sharifullin, A. G., & Dzhamirzoev, G. S. (2016). K voprosu o vysote Bol'shogo (zapadnogo) Sarykuma i prichinakh yeyo izmeneniya za posledneye stoletiye [On the question of the height of the great (western) sarykum and the reasons for its change over the last century]. Proceedings of the state nature reserve “Dagestanskiy”, Makhachkala, 12, 7-16.

Idrisov, I. A. (2010). K istorii formirovaniya i razvitiya peschanogo massiva Sarykum [On the history of the formation and development of the Sarykum sand massif]. Proceedings of the state nature reserve “Dagestanskiy”, Makhachkala, 3, 19-27. In Russian.

Idrisov, I. A. (2011). Lessovidnye porody Dagestana [Loess-like rocks of Dagestan]. Proceeding of Institute of Geology, Dagestan Scientific Centre, RAS, (57), 20-23. In Russian.

Idrisov, I. A. (2013). Relief structure in southwestern Caspian Lowland. Arid ecosystems, 3, 22-27.

Idrisov, I. A. (2014). Rasprostraneniye lessovykh porod v yugo-vostochnom Dagestane [Distribution of loess rocks in the south-east Dagestan]. Young Scientist, (12), 391-396. In Russian.

Kaftan, V. I., Gvishiani, A. D., Manevich, A. I., Dzeboev, B. A., Tatarinov, V. N., Dzeranov, B. V., ... & Losev, I. V. (2024). An Analytical Review of the Recent Crustal Uplifts, Tectonics, and Seismicity of the Caucasus Region. Geosciences, 14(3), 70.

Kazmin, A. S. (2021). Multidecadal variability of the hydrometeorological parameters in the Caspian Sea. Estuarine, Coastal and Shelf Science, 250, 107150.

Koriche, S. A., Nandini-Weiss, S. D., Prange, M., Singarayer, J. S., Arpe, K., Cloke, H. L., ... & Coe, M. (2021a). Impacts of Variations in Caspian Sea Surface Area on Catchment-Scale and Large-Scale Climate. Journal of Geophysical Research: Atmospheres, 126(18), e2020JD034251.

Koriche, S. A., Singarayer, J. S., & Cloke, H. L. (2021b). The fate of the Caspian Sea under projected climate change and water extraction during the 21st century. Environmental Research Letters, 16(9), 094024.

Kostianoy, A. G., Ginzburg, A. I., Lavrova, O. Y., Lebedev, S. A., Mityagina, M. I., Sheremet, N. A., & Soloviev, D. M. (2019). Comprehensive satellite monitoring of Caspian Sea conditions. Remote sensing of the Asian Seas, 505-521.

Krijgsman, W., Tesakov, A., Yanina, T., Lazarev, S., Danukalova, G., Van Baak, C. G., ... & Wesselingh, F. P. (2019). Quaternary time scales for the Pontocaspian domain: Interbasinal connectivity and faunal evolution. Earth-Science Reviews, 188, 1-40.

Kroonenberg, S. B., Rusakov, G. V., & Svitoch, A. A. (1997). The wandering of the Volga delta: a response to rapid Caspian sea-level change. Sedimentary Geology, 107(3-4), 189-209.

Kurbanov, R., Murray, A., Thompson, W., Svistunov, M., Taratunina, N., & Yanina, T. (2021). First reliable chronology for the Early Khvalynian Caspian Sea transgression in the Lower Volga River valley. Boreas, 50(1), 134-146.

Kurbanov, R.N., Belyaev, V.R., Svistunov, M.I., Butuzova, E.A., Solodovnikov, D.A., Taratunina, N.A., Yanina, T.A. (2023). New data on the age of the early Khvalynian transgression of the Caspian Sea. Izvestiya Rossiyskoy Akademii Nauk, Seriya Geograficheskaya V 87, 403–419. In Russian.

Kurbanov, R. N., Buylaert, J. P., Stevens, T., Taratunina, N. A., Belyaev, V. R., Makeev, A. O., ... & Yanina, T. A. (2022). A detailed luminescence chronology of the Lower Volga loess-palaeosol sequence at Leninsk. Quaternary Geochronology, 73, 101376.

Költringer, C., Bradák, B., Stevens, T., Almqvist, B., Banak, A., Lindner, M., ... & Snowball, I. (2021). Palaeoenvironmental implications from Lower Volga loess-Joint magnetic fabric and multi-proxy analyses. Quaternary Science Reviews, 267, 107057.

Leroy, S. A., Gracheva, R., & Medvedev, A. (2022). Natural hazards and disasters around the Caspian Sea. Natural Hazards, 114(3), 2435-2478.

Lokhin, M.Yu., Maev, E.G. (1990) Pozdnepleistotsenovye delty na shelfe severnoi chasti Srednego Kaspiya [Late Pleistocene deltas on the shelf of the northern part of the Middle Caspian Sea]. Vestnik Moskovskogo Universiteta. Seria 5 Geografia, 3, 34-40. In Russian.

Lukk, A. A., & Sidorin, A. Y. (2022). The 1970 Dagestan Earthquake a Half-Century Later. Seismic Instruments, 58(Suppl 1), S123-S134.

Maev, E. G. (2009). Stages of the Mangyshlak regression of the Caspian Sea. Vestnik Moskovskogo universiteta. Seria Geografia 1, 15-20. In Russian.

Maiorov, A.A. (1927). Eolovaya pustynya u podnozhiya Dagestana [Aeolian desert near the Dagestan piedmont]. DagNII, 116 pp. In Russian.

Makshaev, R. R., & Tkach, N. T. (2022). Chronology of Khvalynian stage of the Caspian Sea according to radiocarbon dating. In Doklady Earth Sciences (Vol. 507, No. Suppl 1, pp. S51-S60). Moscow: Pleiades Publishing.

Matsapulin, V. U., Tulysheva, E. V., & Khlopkova, M. V. (2013). Geological conditions of sandy Sarykum barkhan formation and geochemical features of its carbonate deposits. Arid ecosystems, 3, 10-15.

Matsapulin, V. U., Tulysheva, E.V., Isakov, S.I. (2021). Karbonatnye korochki-paleogeizerity v eolovykh peskakh dyuny Sarykum Dagestana (Vostochnyi Kavkaz) [Carbonated crusts–paleogeyserites in aeolian sands of the Sarukum dune of Dagestan (East Caucausus)]. Monitoring. Science and technology, (3), 6-10. In Russian.

Murray, A. S., & Wintle, A. G. (2003). The single aliquot regenerative dose protocol: potential for improvements in reliability. Radiation measurements, 37(4-5), 377-381.

Over, J. S. R., Ritchie, A. C., Kranenburg, C. J., Brown, J. A., Buscombe, D. D., Noble, T., ... & Wernette, P. A. (2021). Processing coastal imagery with Agisoft Metashape Professional Edition, version 1.6—Structure from motion workflow documentation (No. 2021-1039). US Geological Survey.

Pearce, K. I., & Walker, I. J. (2005). Frequency and magnitude biases in the 'Fryberger'model, with implications for characterizing geomorphically effective winds. Geomorphology, 68(1-2), 39-55.

Popov, G.I., 1983. Pleistocen Chernomorsko-Kaspijskikh Prolivov [Pleistocene of the Black Sea – Caspian Sea Passages]. Nauka Press, Moscow, p. 216 (in Russian).

Prescott, J. R., & Hutton, J. T. (1994). Cosmic ray contributions to dose rates for luminescence and ESR dating: large depths and long-term time variations. Radiation measurements, 23(2-3), 497-500.

Richards, K., Bolikhovskaya, N. S., Hoogendoorn, R. M., Kroonenberg, S. B., Leroy, S. A., & Athersuch, J. (2014). Reconstructions of deltaic environments from Holocene palynological records in the Volga delta, northern Caspian Sea. The Holocene, 24(10), 1226-1252.

Ryabogina, N., Borisov, A., Idrisov, I., & Bakushev, M. (2019). Holocene environmental history and populating of mountainous Dagestan (Eastern Caucasus, Russia). Quaternary International, 516, 111-126.

Ryabogina, N. E., Idrisov, I. A., Yuzhanina, E. D., & Borisov, A. V. (2022). Peat palaeorecords from the arid Caspian Lowland in Russia: Environmental and anthropogenic effects during the second half of the Holocene. Quaternary Science Reviews, 280, 107417.

Rychagov, G.I. (1997). Pleistotsenovaya istoriya Kaspiya [Pleistocene History of the Caspian Sea]. Moscow State University, Moscow, pp. 1-267. In Russian.

Shakhovets, S.A. (1987). Khronologiya paleogeographicheskikh sobytii pozdnego pleistotsena Nizhnei Volgi (po dannym termolyuministsentnogo metoda) [Chronology of the Late

Pleistocene paleogeographic events of the Lower Volga region (based on thermoluminiscence method)]. PhD thesis, Moscow State University. In Russian.

Sobornov, K. (2021). Structure and evolution of the Terek-Caspian fold-and-thrust belt: New insights from regional seismic data. Journal of Petroleum Geology, 44(3), 259-286.

Svitoch, A.A., Yanina, T.A. (1997). Chetvertichnye Otlozheniya Poberezhiy Kaspijskogo Moria [Quaternary Deposits of the Caspian Sea Coasts]. RASKhN Press, Moscow. In Russian.

Svitoch, A.A., Klyuvitkina, T.S. (2006). Baerovskiye Bugry Nizhnego Povolzh'ya [Baer Knolls from the Lower Volga Region]. Faculty of Geography, Moscow State University (in Russian).

Svitoch, A. A. (2007). On the nature of the Khvalynian transgression of the Caspian Sea. Oceanology, 47, 282-289.

Taratunina, N., Rogov, V., Streletskaya, I., Thompson, W., Kurchatova, A., Yanina, T., & Kurbanov, R. (2021). Late Pleistocene cryogenesis features of a loess-paleosol sequence in the Srednyaya Akhtuba reference section, Lower Volga River valley, Russia. Quaternary International, 590, 56-72.

Taratunina, N. A., Buylaert, J. P., Kurbanov, R. N., Yanina, T. A., Makeev, A. O., Lebedeva, M. P., ... & Murray, A. S. (2022). Late Quaternary evolution of lower reaches of the Volga River (Raygorod section) based on luminescence dating. Quaternary Geochronology, 72, 101369.

Taratunina, N., Buylaert, J. P., Murray, A., Yanina, T., Streletskaya, I. D., & Kurbanov, R. (2024). Luminescence dating of Late Pleistocene sea level change and cryogenesis in the northern Caspian region (Chernyy Yar section). Quaternary Geochronology, 82, 101538.

Tatarinov, V. N., Kaftan, V. I., Manevich, A. I., Dzeboev, B. A., Dzeranov, B. V., Avdonina, A. M., ... & Korol'kovaa, A. A. (2024). Neotectonic evolution of the Caucasus: recent vertical movements and mechanism of crustal deformation. Fizika zemli, (4), 76-99.

Thiel, C., Buylaert, J. P., Murray, A., Terhorst, B., Hofer, I., Tsukamoto, S., & Frechen, M. (2011). Luminescence dating of the Stratzing loess profile (Austria)–Testing the potential of an elevated temperature post-IR IRSL protocol. Quaternary International, 234(1-2), 23-31.

Volkov, I.A. (1960). O geologicheskom stroenii i relyefe bugrov Baera [On the geological structure and relief of the Baer Knolls]. Aeromethods in natural research (proceedings of the laboratory of aeromethods of AS USSR). Moscow, 74-89.

Volozh, Y. A., Gogonenkov, G. N., Guliev, I. S., Dmitrievsky, A. N., Kuandykov, B. M., Miletenko, N. V., ... & Fedonkin, M. A. (2022). Geological Aspects of Energy and Environmental-Safety Problems in the Caspian Region. Russian Geology and Geophysics, 63(3), 255-264.

Vyruchalkina, T. Y., Dianskii, N. A., & Fomin, V. V. (2020). Effect of long-term variations in wind regime over Caspian Sea Region on the evolution of its level in 1948–2017. Water Resources, 47, 348-357.

Wintle, A. G. (1997). Luminescence dating: laboratory procedures and protocols. Radiation measurements, 27(5-6), 769-817.

Yanina, T.A., 2009. Paleogeografiya basseynov Ponto-Kaspia v pleystotsene porezul’tatam malakofaunisticheskogo analiza [Paleogeography of the Ponto-Caspian basins in the Pleistocene based on the results of malacofaunistic analysis]. In: Avtoref. Dokt. Geograf. Nauk. Moscow State University, Moscow, p. 42.In Russian.

Yanina, T. A. (2014). The Ponto-Caspian region: Environmental consequences of climate change during the Late Pleistocene. Quaternary International, 345, 88-99.

Yanina, T., Bolikhovskaya, N., Sorokin, V., Romanyuk, B., Berdnikova, A., & Tkach, N. (2021). Paleogeography of the Atelian regression in the Caspian Sea (based on drilling data). Quaternary International, 590, 73-84.

Zastrozhnov, A. S., Danukalova, G. A., Golovachev, M. V., Titov, V. V., Tesakov, A. S., Simakova, A. N., ... & Kurmanov, R. G. (2018). Singil deposits in the Quaternary scheme of the lower Volga region: new data. Stratigraphy and Geological Correlation, 26, 659-697.

Zastrozhnov, A., Danukalova, G., Golovachev, M., Titov, V., Osipova, E., Simakova, A., ... & Sadikhov, E. (2020). Biostratigraphical investigations as a tool for palaeoenvironmental reconstruction of the Neopleistocene (Middle-Upper Pleistocene) at Kosika, Lower Volga, Russia. Quaternary International, 540, 38-67.

Zastrozhnov, A., Danukalova, G., Golovachev, M., Osipova, E., Kurmanov, R., Zenina, M., ... & Gimranov, D. (2021). Pleistocene palaeoenvironments in the Lower Volga region (Russia): Insights from a comprehensive biostratigraphical study of the Seroglazovka locality. Quaternary International, 590, 85-121.

Zastrozhnov, A., Danukalova, G., Osipova, E., Kurmanov, R., Lazarev, S., & Zastrozhnov, D. (2024). Caspian transgressive-regressive cycles across the Lower Volga region during the

Quaternary reconstructed from the borehole at Ulan-Khol (Kalmykia, Russia). Quaternary International, 686, 99-119.